

University of Windsor

## Scholarship at UWindor

---

Electronic Theses and Dissertations

Theses, Dissertations, and Major Papers

---

2012

# Control Oriented NOx and Soot Emission Estimation for Diesel Engine

Fangfang Lin  
*University of Windsor*

Follow this and additional works at: <https://scholar.uwindsor.ca/etd>

---

### Recommended Citation

Lin, Fangfang, "Control Oriented NOx and Soot Emission Estimation for Diesel Engine" (2012). *Electronic Theses and Dissertations*. 5368.

<https://scholar.uwindsor.ca/etd/5368>

This online database contains the full-text of PhD dissertations and Masters' theses of University of Windsor students from 1954 forward. These documents are made available for personal study and research purposes only, in accordance with the Canadian Copyright Act and the Creative Commons license—CC BY-NC-ND (Attribution, Non-Commercial, No Derivative Works). Under this license, works must always be attributed to the copyright holder (original author), cannot be used for any commercial purposes, and may not be altered. Any other use would require the permission of the copyright holder. Students may inquire about withdrawing their dissertation and/or thesis from this database. For additional inquiries, please contact the repository administrator via email ([scholarship@uwindsor.ca](mailto:scholarship@uwindsor.ca)) or by telephone at 519-253-3000ext. 3208.

# **Control Oriented NO<sub>x</sub> and Soot Emission Estimation for Diesel Engine**

by

Fangfang Lin

A Thesis

Submitted to the Faculty of Graduate Studies  
through the Department of Mechanical, Automotive, and Materials Engineering  
in Partial Fulfillment of the Requirements for  
the Degree of Master of Applied Science at the  
University of Windsor

Windsor, Ontario, Canada

2011

© 2011 Fangfang Lin

Control oriented NOx and Soot Emission Estimation for Diesel Engine

by

Fangfang Lin

APPROVED BY:

---

Dr. Beham Shahrrava, Outside Departmental Reader  
Department of Electrical and Computer Engineering

---

Dr. David Ting, Departmental Reader  
Department of Mechanical, Automotive and Materials Engineering

---

Dr. Ming Zheng, Advisor  
Department of Mechanical, Automotive and Materials Engineering

---

Dr. Xiang Chen, Advisor  
Department of Electrical and Computer Engineering

---

Dr. Vesselin Stoilov, Chair of Defense  
Department of Mechanical, Automotive and Materials Engineering

Dec.16, 2011

---

## **DECLARATION OF ORIGINALITY**

I hereby certify that I am the sole author of this thesis and that no part of this thesis has been published or submitted for publication.

I certify that, to the best of my knowledge, my thesis does not infringe upon anyone's copyright nor violate any proprietary rights and that any ideas, techniques, quotations, or any other material from the work of other people included in my thesis, published or otherwise, are fully acknowledged in accordance with the standard referencing practices. Furthermore, to the extent that I have included copyrighted material that surpasses the bounds of fair dealing within the meaning of the Canada Copyright Act, I certify that I have obtained a written permission from the copyright owner(s) to include such material(s) in my thesis and have included copies of such copyright clearances to my appendix.

I declare that this is a true copy of my thesis, including any final revisions, as approved by my thesis committee and the Graduate Studies office, and that this thesis has not been submitted for a higher degree to any other University or Institution.

---

## ABSTRACT

Comparing to conventional Electric Vehicles (EVs) and Hybrid Electric Vehicles (HEV), Plug-in Hybrid Electric Vehicles (PHEVs) have gained more attraction from researchers due to their advantages of extended all-electric range, decreased emission and being less dependent on recharging infrastructure. In order to develop power control and management for diesel engine-generator set in a series PHEV system, an estimation mechanism based on the NO<sub>x</sub> and soot emission with the impact of Exhaust Gas Recirculation (EGR) is developed in this thesis. In particular, the single zone combustion thermodynamic engine sub-model, NO<sub>x</sub> estimation sub-model (based on extended Zeldovich mechanism), soot estimation sub-model (based on Hiroyasu's two-step empirical model) and EGR sub-model are incorporated together. In order to illustrate the impact of EGR on the NO<sub>x</sub> and soot emission, the EGR sweep experiment has been carried out under certain working conditions. And, the simulation results have been validated with the empirical data. Finally, based on the validation of the emission estimation mechanism and the selected eight operating points working condition, the results EGR sweep results have been generated for the series PHEV engine-generator control design. In general, the present work targets on estimating real-time NO<sub>x</sub> and soot emission based on the inputs information, such as intake boost, fuel injection, injection timing etc, and the purpose of this thesis is to aid development of engine emission management with study about the effect of EGR on the reduction and the soot trade-off.

Key words: diesel emission estimation, PHEVs, thermodynamic engine model, EGR;

---

## DEDICATION

*To my beloved,*

*Adrian Wydra*

---

## ACKNOWLEDGEMENTS

I would like to thank my supervisors, Dr. Xiang Chen and Dr. Ming Zheng, for their genuine guiding and encouragement during this work.

I would also like to thank my committee members Dr. David Ting and Dr. Behnam Shahrava for their advice in my research.

My gratitude will also be directed towards my colleagues in Clean Diesel Engine Laboratory and Advanced Control System Laboratory: Dr. Meiping Wang for her kind help in my personal life and guidance in my lab work; Dr. Yu for his constant guidance; Xiaoye Han, Xiaoxi Zhang, Kelvin Xie for their help in the experiment work and helpful discussion; Grignion Danny and Prasad Divekar for their kind help on proposal and thesis writing; Qiaochu Han for her support and friendship.

Ultimately, I would like to express my gratitude to my parents, my brother and my fiancé Adrian Wydra for their support and love. Without their patience and love, I would never accomplish this work.

---

# TABLE OF CONTENTS

|   |      |
|---|------|
| DECLARATION OF ORIGINALITY .....  | III  |
| ABSTRACT.....   | IV   |
| DEDICATION .....  | V    |
| ACKNOWLEDGEMENTS .....  | VI   |
| LIST OF TABLES .....  | VIII |
| LIST OF FIGURES .....   | IX   |
| CHAPTER 1 INTRODUCTION .....  | 1    |
| 1.1 Diesel Engine Emission Estimation.....                              | 1    |
| 1.2 Literature Review .....   | 4    |
| 1.3 Research Objectives.....  | 6    |
| CHAPTER 2 BACKGROUND .....  | 9    |
| 2.1 Combustion Model.....   | 13   |
| 2.2 Heat Release Model .....  | 16   |
| 2.3 Heat Transfer Model .....   | 18   |
| 2.4 EGR System.....   | 19   |
| CHAPTER 3 CONTROL ORIENTED NO <sub>x</sub> AND SOOT ESTIMATION .....    | 22   |
| 3.1 NO <sub>x</sub> Emission Estimation.....                            | 22   |
| 3.2 Soot Emission Estimation .....                                      | 24   |
| CHAPTER 4 EXPERIMENT SETUP AND ESTIMATION RESULT VALIDATION .....       | 27   |
| 4.1 Experiment Setup.....   | 27   |
| 4.2 Estimation Result Validation .....                                  | 28   |
| CHAPTER 5 APPLICATION OF ESTIMATION RESULTS TO SMART DIESEL ENGINE..... | 42   |
| CHAPTER 6 CONCLUSION AND FUTURE WORK .....                              | 54   |
| 6.1 Conclusion .....  | 54   |
| 6.2 Future Work.....  | 54   |
| REFERENCES .....  | 56   |
| APPENDIX A. ESTIMATION RESULT VALIDATION.....                           | 63   |
| VITA AUCTORIS .....   | 67   |



---

## LIST OF TABLES

|  |    |
|--|----|
| TABLE 4- 1 SINGLE CYLINDER RESEARCH ENGINE GEOMETRICAL SPECIFICATION ..... | 30 |
| TABLE 5- 1 SMART ENGINE SPECIFICATION .....                                | 42 |
| TABLE 5- 2 DETAILED INFORMATION ABOUT 8 OPERATING POINTS.....              | 44 |

---

## LIST OF FIGURES

|  |    |
|--|----|
| FIGURE 1- 1 TYPICAL DIRECT IGNITION (DI) DIESEL ENGINE HEAT RELEASE RATE<br>DIAGRAM .....        | 3  |
| FIGURE 1- 2 EUROPEAN NOX AND PM EMISSIONS STANDARD FOR HEAVY-DUTY<br>DIESEL ENGINE .....         | 4  |
| FIGURE 1- 3 SERIES PHEV POWERTRAIN SYSTEM .....  | 7  |
| FIGURE 1- 4 NOX AND SOOT EMISSION ESTIMATION BLOCK.....  | 8  |
| FIGURE 2- 1 ENGINE BRAKE SPECIFIC FUEL CONSUMPTION CONTOUR .....                                 | 11 |
| FIGURE 2- 2 THERMODYNAMIC ENGINE MODEL AND EMISSION ESTIMATION<br>MODEL .....                    | 13 |
| FIGURE 2- 3 THERMODYNAMIC ENGINE MODEL.....  | 15 |
| FIGURE 4- 1 SINGLE CYLINDER RESEARCH ENGINE TEST PLATFORM .....                                  | 27 |
| FIGURE 4- 2 HEAT RELEASE RATE WITH DIFFERENT M VALUE.....  | 31 |
| FIGURE 4- 3 BURN RATES FOR CONSTANT COMBUSTION DURATION AND<br>DIFFERENT VALUES OF M .....       | 31 |
| FIGURE 4- 4 COMPARISON OF THE CALCULATED AND EXPERIMENTAL<br>IN-CYLINDER PRESSURE (EGR=21%)..... | 32 |
| FIGURE 4- 5 COMPARISON OF HEAT RELEASE RATE FROM EXPERIMENT AND<br>SIMULATION (EGR=21%).....     | 33 |
| FIGURE 4- 6 AVERAGE IN-CYLINDER TEMPERATURE (EGR=21%).....                                       | 34 |
| FIGURE 4- 7 COMPARISON OF THE CALCULATED AND MEASURED IN-CYLINDER                                |    |

---

|  |    |
|--|----|
| PRESSURE (EGR=34%) .....   | 35 |
| FIGURE 4- 8 COMPARISON OF HEAT RELEASE RATE FROM EXPERIMENT AND<br>SIMULATION (EGR=34%).....                 | 36 |
| FIGURE 4- 9 AVERAGE IN-CYLINDER TEMPERATURE (EGR=34%).....   | 36 |
| FIGURE 4- 10 SPECIES (O <sub>2</sub> , CO <sub>2</sub> AND H <sub>2</sub> O ) MOLE FRACTION (EGR=34%).....   | 37 |
| FIGURE 4- 11 SPECIES (O <sub>2</sub> , CO <sub>2</sub> , AND H <sub>2</sub> O) MOLE FRACTION (EGR=21%) ..... | 38 |
| FIGURE 4- 12 CALCULATED AND MEASURED IN-CYLINDER NITRIC OXIDE (NO)<br>CONCENTRATION .....                    | 39 |
| FIGURE 4- 13 CALCULATED AND MEASURED IN-CYLINDER SOOT<br>CONCENTRATION .....                                 | 39 |
| FIGURE 4- 14 CALCULATED AND MEASURED IN-CYLINDER NITRIC OXIDE (NO)<br>FORMATION .....                        | 40 |
| FIGURE 4- 15 CALCULATED AND MEASURED IN-CYLINDER NITRIC OXIDE (NO)<br>FORMATION .....                        | 41 |
| FIGURE 5- 1 SMART CAR CDI ENGINE .....   | 43 |
| FIGURE 5- 2 PHOTO OF ENGINE-GENERATOR SET (COURTESY RICARDO).....  | 43 |
| FIGURE 5- 3 RELATIONSHIP BETWEEN EGR AND NOX FORMATION (FOR<br>OPERATING POINT 1-4).....                     | 45 |
| FIGURE 5- 4 RELATIONSHIP BETWEEN EGR AND NOX FORMATION (FOR<br>OPERATING POINT 5-7).....                     | 46 |
| FIGURE 5- 5 RELATIONSHIP BETWEEN EGR AND NOX FORMATION (FOR<br>OPERATING POINT 8) .....                      | 47 |
| FIGURE 5- 6 RELATIONSHIP BETWEEN EGR AND SOOT DENSITY (FOR OPERATING   |    |

---

|  |    |
|--|----|
| POINT 1-4) .....   | 48 |
| FIGURE 5- 7 RELATIONSHIP BETWEEN EGR AND SOOT DENSITY (FOR OPERATING<br>POINT 5-7) .....       | 48 |
| FIGURE 5- 8 RELATIONSHIP BETWEEN EGR AND SOOT DENSITY (FOR OPERATING<br>POINT 8) .....         | 49 |
| FIGURE 5- 9 IN-CYLINDER TRACES WITH DIFFERENT EGR RATES (OPERATING<br>POINT 3) .....           | 50 |
| FIGURE 5- 10 IN-CYLINDER TRACES WITH DIFFERENT EGR RATES (OPERATING<br>POINT 8) .....          | 50 |
| FIGURE 5- 11 HEAT RELEASE RATE WITH DIFFERENT EGR RATES (OPERATING<br>POINT 3) .....           | 51 |
| FIGURE 5- 12 EFFECT OF BOOST ON IGNITION DELAY .....   | 52 |
| FIGURE 5- 13 EFFECT OF INTAKE OXYGEN CONCENTRATION ON THE IN-CYLINDER<br>PEAK PRESSURE .....   | 53 |
| FIGURE A- 1 COMPARISON OF THE CALCULATED AND MEASURED IN-CYLINDER<br>PRESSURE (EGR=6.5%) ..... | 63 |
| FIGURE A- 2 COMPARISON OF THE CALCULATED AND MEASURED IN-CYLINDER<br>PRESSURE (EGR=12%) .....  | 64 |
| FIGURE A- 3 COMPARISON OF THE CALCULATED AND MEASURED IN-CYLINDER<br>PRESSURE (EGR=15%) .....  | 64 |
| FIGURE A- 4 COMPARISON OF THE CALCULATED AND MEASURED IN-CYLINDER<br>PRESSURE (EGR=25%) .....  | 65 |
| FIGURE A- 5 COMPARISON OF THE CALCULATED AND MEASURED IN-CYLINDER                              |    |

---

|   |    |
|---|----|
| PRESSURE (EGR=30%) .....  | 65 |
| FIGURE A- 6 COMPARISON OF THE CALCULATED AND MEASURED IN-CYLINDER |    |
| PRESSURE (EGR=35%) .....  | 66 |

---

## NOMENCLATURE

|      |                                   |
|------|-----------------------------------|
| BSFC | Break Specific Fuel Consumption   |
| CA   | Crank Angle                       |
| EGR  | Exhaust Gas Recirculation         |
| EV   | Electric Vehicle                  |
| FSN  | Filter Smoke Number               |
| HEV  | Hybrid Electric Vehicle           |
| HRR  | Heat Release Rate                 |
| ID   | Ignition Delay                    |
| IMEP | Indicated Mean Effective Pressure |
| L    | Liter                             |
| NO   | Nitric Oxide                      |
| RPM  | Revolution per Minute             |
| TDC  | Top Dead Center                   |
| PHEV | Plug-in Hybrid Electrical Vehicle |
| Pinj | Injection Pressure                |
| RPM  | Revolution Per Minute             |
| SOC  | Start of Combustion               |
| SOI  | Start of Injection                |
| Tw   | Cylinder Wall Temperature         |

## CHAPTER 1 INTRODUCTION

Due to the increasing oil price and stringent regulations on emissions around the globe, Electric Vehicles (EVs) and Hybrid Electric Vehicles (HEVs) [1] have received much research attention in the past few decades. Recently, many studies have been carried out in the field of Plug-in Hybrid Electric Vehicles (PHEVs) [3][4], which are considered as the new generation of HEV, because of rapidly improving battery technology. Gasoline engine (or other spark-ignition engine) equipped with an electric motor is still the most popular hybrid powertrains [5]. Comparing with conventional gasoline engine and HEVs, gasoline PHEVs reduce CO<sub>2</sub> emissions by 37%-67% and 19-54% [6]. But being encouraged by the Diesel engine (also known as compression-ignited engine) fuel economy benefits and high engine performance potential under low speed condition, researchers have increasing interests in the development of combination of diesel engines and electric motor in HEVs and PHEVs. Especially in Europe, automakers such as Volvo, Mercedes-Benz and Volkswagen are paying much attention to the investigation of diesel PHEVs.

### 1.1 Diesel Engine Emission Estimation

Emissions from internal combustion engine are released to the environment mainly into air and sometimes it is absorbed in water in marine application. The impact of air pollution is significant and few areas around the world are not impacted by its effects. Road transportation is considered a significant contributor to air pollution in cities. It's the main contributor for the emission of nitrogen dioxide. In recent decades, the epidemiological and toxicological evidence on the

effects of transport-related air pollution on health has increased heavily [6]. The National Pollutant Inventory Guide list and detailed the four types of emission estimation techniques, which are sampling or direct measurement, mass balance, fuel analysis or other engineering calculations and emissions factors [10].

Since an early successful diesel engine was demonstrated by Rudolph Diesel at the 1900 Paris Exhibition [8], this technology has changed the world. High compression ratio and lean fuel running condition bring the high thermal efficiencies to Diesel engine. Comparing with gasoline engine, today's turbocharged diesel engine has 30% better fuel economy [8]. The most difficult challenges for diesel engine designers are the formation of soot particles and NO<sub>x</sub>. When the high velocity injected diesel fuel is directly sprayed into the air in the main combustion chamber, which is compressed to a high temperature and pressure, it vaporizes quickly and mixes with the air. Without spark plug applied, the mixture is ignited after undergoing a series of chemical reactions. Because the fuel distribution is non-uniform, NO<sub>x</sub> forms in the high flame temperature area, and the highest formation rate is in the close-to-stoichiometric regions [9]. The soot particles are generated from the incomplete combustion of hydrocarbon fuel because of the highly non-homogeneous environment. Over the past few years, due to the imposed emission regulations, extraordinary achievements of developing clean diesel engine have been made when new techniques are utilized such as common rail system, fuel injection control strategies, exhaust gas recirculation and exhaust gas after treatment etc [12].



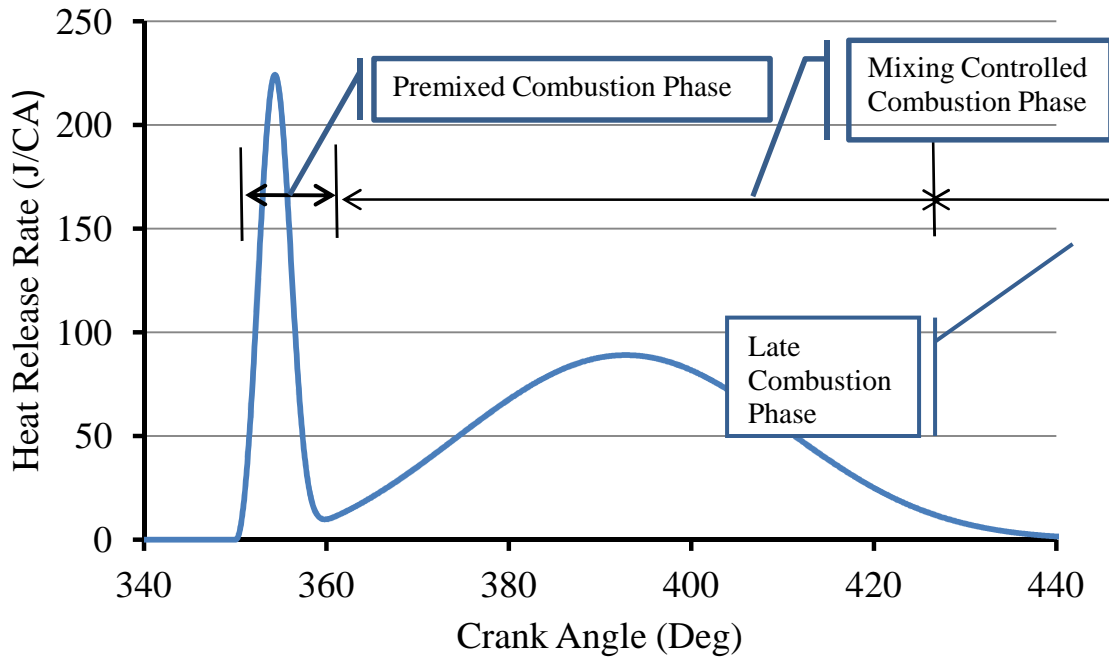


Figure 1- 1 Typical Direct Ignition (DI) Diesel Engine Heat Release Rate Diagram

To order to predict the engine performance and NO<sub>x</sub> and soot emission formation, it is necessary and important to understand the details of diesel engine combustion process [1]. For Diesel engine, the pollutant formation processes are mainly determined by fuel mixture distribution in the cylinder. Figure 1- 1 shows the typical Direct Ignition (DI) Diesel engine heat release rate diagram. After the ignition delay period, the fuel combustion takes place rapidly with the high heat-release rate during the premixed combustion phase.

To cope with the air pollution problem, stringent emission limits have been implemented to diesel engine. The following diagrams Figure 1- 2 show the European Emission Standards for HD Diesel Engine with respect to NO<sub>x</sub> and soot emission ranging from the 1992 to 2013. These two diagrams reveal the restriction of the emission standard over time. For example, the

concentrations in 2013 are expected to be roughly 25% of those in 2008.

An estimation of Diesel engine emission is essential for the Diesel engine-generator set control design. The real diesel engine works as a highly non-linear mechanical system [14], it is extremely hard to produce a model with truly predictive capabilities to achieve more precise estimation. With the rapid development of microprocessor technology, these engines models can be applied in the field of real-time state estimation, control and fault diagnostics [15][16]. Early efforts in diesel engine modeling were focus on specific closed part of the engine cycle, and the linear dynamic models were developed based on the usage of empirical data [17][2]. The great drawbacks of these quasi-linear models are their huge dependence on the empirical data, which need to be collected prior to the simulations, and poor performance to the transient response.

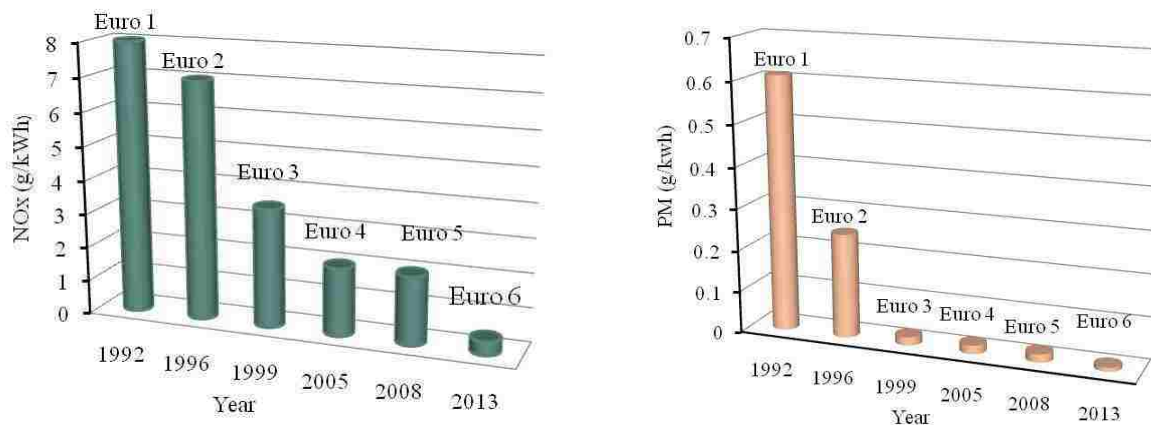


Figure 1- 2 European NOx and PM Emissions Standard for Heavy-Duty Diesel Engine

## 1.2 Literature Review

Nowadays, most of the phenomena related to combustion have been revealed by empirical study.

---

However, there is no experimental equipment or technique which can provide and clarify all detailed relevant chemical reactions. Based on the understanding of chemical processes, the simulation modeling and analysis investigation is necessary.

NO<sub>x</sub> emissions consists of NO and NO<sub>2</sub>. The NO<sub>2</sub> formation is via the oxidation of NO. Therefore, the simulation of NO<sub>x</sub> formation is reduced to understanding of NO formation [21]. Based on the mechanism developed by Ahmed and Plee [17] that the majority of NO formation is via thermal path, Zeldovich mechanism and extended Zeldovich mechanism were postulated by Zeldovich and further developed by Lavoie [9]. The empirical heat transfer correlation was utilized in these phenomenological models. Miller et al [18] and Sundar R. Krishnan *et al* [19] improved the mechanism to super extended Zeldovich mechanism. Sundar R. Krishnan *et al*'s model accounts for 43 reactions and 20 species and Miller *et al*'s model includes 67 reactions and 13 species ,which provided more accurate prediction results, instead of the typical three reactions used in the extended Zeldovich mechanism. But then more reactions and species are included in the calculation results in higher computational complexity.

Although the soot formation phenomenon in the in-cylinder turbulent spray combustion is far from being fully understood, various models have been developed for soot predictions [21]. Khan and Greees first presented the model for the prediction of soot for diesel engines. Later on, detailed kinetic soot models were proposed [22] to describe soot dynamic formation. Complex gas phase chemistry reaction and particle growth and distribution were considered in detailed kinetic approach. Due to the complexity of turbulence, thermochemistry, and the appearance of Arrheius terms in detailed kinetic models, there have been concerns about using this approach to

simulate diesel combustion condition. Hiroyasu et al. proposed a two-step phenomenological model to predict soot formation distribution [23] for combustion engines. Because Hiroyasu's model is easy to be implemented into CFD simulation code, most of the modern prediction of soot formation for multidimensional diesel engine calculation was based on this empirical approach. Comparing to the detailed kinetic soot model, the phenomenological model consists one Arrhenius term in the soot formation step with two empirical constants and the particle growth and the dynamic of soot has not been taken into account. Niklas Winkler [25] incorporated a multi-zone diesel engine model for NO<sub>x</sub> prediction with a simplified soot formation estimation model, which were tuned with constant parameters during the entire engine operating range. The calculated engine performance which was produced from a 1-dimensional fluid dynamic code GT-Power for transient operation was validated with the experimental data.

### **1.3 Research Objectives**

Figure 1-1 represents the clean diesel series plug-in hybrid electrical vehicle (PHEV) powertrain system. The author has been working on this project with other colleague at Clean Diesel Engine Laboratory. As shown in Figure 1-3, the development of the Diesel Engine model and the real time emission estimation model have been carried out by the author. The series HEVs proposed in this thesis has three power sources: the primary power sources are the high voltage battery and the super capacitors while the assistant power source is the diesel -generator set.

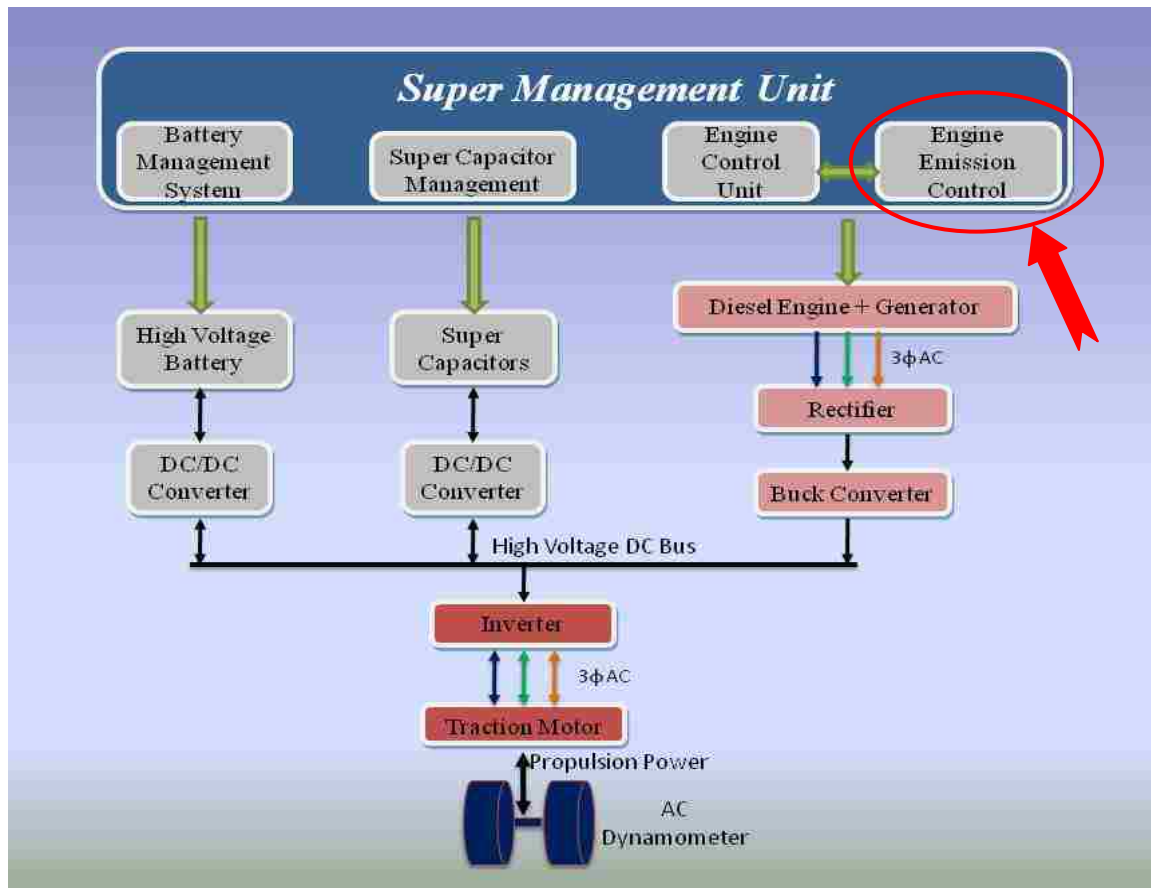


Figure 1- 3 Series PHEV Powertrain System

The main goal of this thesis is developing an engine thermodynamic model and emission (NO<sub>x</sub> and Soot) estimation for a smart engine, incorporating of the EGR model into the engine model and the validation of the engine and emission estimation. The proposed single dimensional engine thermodynamic model provides the in-cylinder pressure, temperature, heat release rate (HRR), species fraction during the combustion process. Sub-models include:

- 1) Ignition delay model
- 2) Heat release model
- 3) Heat transfer model

These models are integrated together to predict engine performance and estimate emission formation. At the end of the thesis, the calculation results of the 8 operating points for the smart engine are also included.

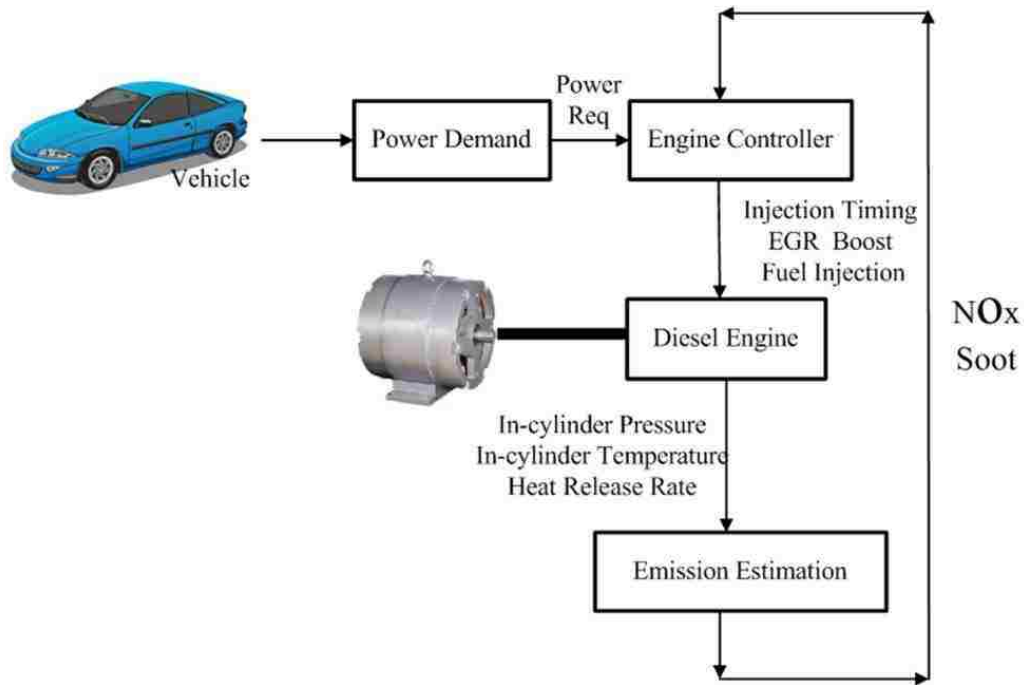


Figure 1- 4 NOx and Soot Emission Estimation Block

## CHAPTER 2 BACKGROUND

PHEVs are a potentially important technology for reducing the fossil fuel consumption and CO<sub>2</sub> emission because they can run on electricity for a certain distance after each recharge, depending on their battery's energy storage capacity, which is expected to be typically between 20km and 80km [1]. PHEVs offer great promise for petroleum displacement [29]. According to the 2009 National Household Travel Survey [28], in 2009, people travels 36.1 miles per day and average daily trips per person is 3.8. Although PHEVs will be more expensive than conventional and hybrid vehicles, the cost can be recovered by fuel saving. Meanwhile, people will benefit from emissions reduction.

The powertrain configurations include series, parallel and power split vehicle configurations. Comparing with other configurations, the series engine configuration is often considered to be closer to a pure electric vehicle. Since engine operation is directly related to fuel efficiency and gaseous emissions, it plays an important part in the hybrid vehicle control strategy [30][27].

Engine operating point is one of the important parameters affecting the vehicle control strategy. Engine operating point is directly related to fuel efficiency and emissions [31]. As mentioned before in Fig 1-2, in the case of series PHEVs configuration, the propulsion power for the vehicle is exclusively coming from the electrical energy source traction motor. As a result of that, engine speed is entirely decoupled from the wheel axles, and the engine operation point is independent of vehicle operations [31]. From the diesel engine perspective, as shown in Fig 2-1 the brake

specific fuel consumption (BSFC) curve, with the characteristic series PHEVs system, diesel engine can work along the best efficiency curve while satisfying the power demand. Meanwhile, when the diesel engine works in the optimal engine operating points, NO<sub>x</sub> and PM emission increase dramatically. It brings another challenging constraint in the control strategy.

In the Argonne National Laboratory, Maxime research group conducted the project to test the effect of powertrain system control on diesel engine emissions and fuel efficiency, based on the conventional diesel engine and PHEVs. The trade-off relation between fuel economy and emission from different configurations was studied; however, the NO<sub>x</sub> and PM emission was not considered as one of the constraints in the control theory in simulation models. Aymeric Rousseau [29] tested the fuel efficiency of power split and series configuration midsize vehicles on more than real world driving conditions cycles. In Oak Ridge National Laboratory, Vehicle Technologies Program started the advanced PHEV Engine Systems and Emissions Control Modeling and Analysis program in 2005. One of the project objectives is to apply the simulation to test the fuel efficiency and emissions impact of advanced combustion (HCCI, PCCI) versus conventional SI and diesel engines.



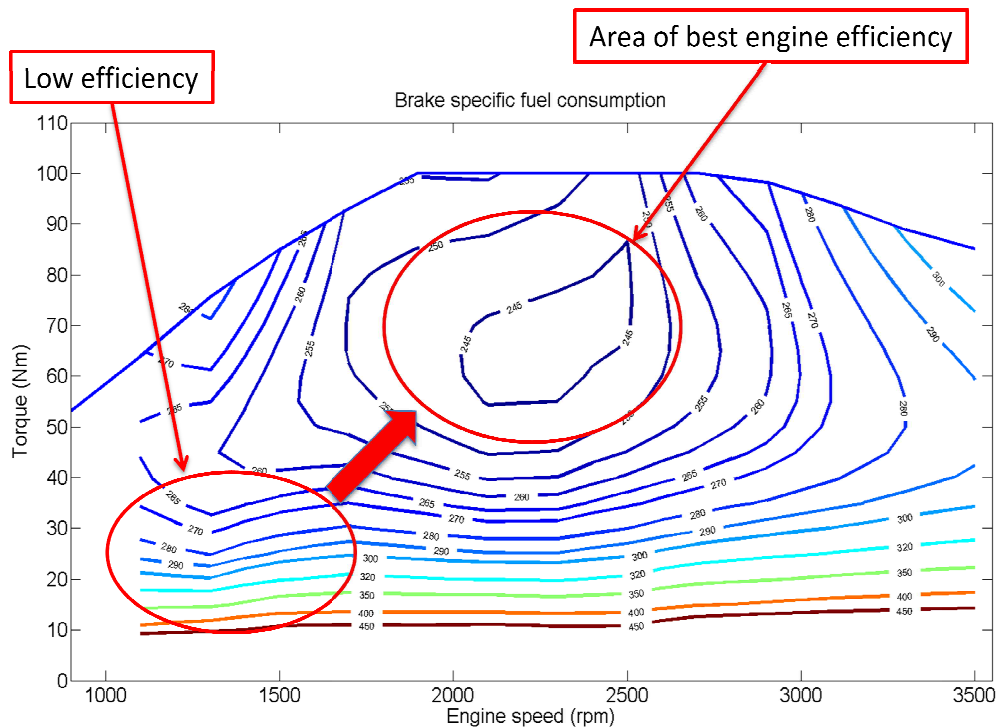


Figure 2- 1 Engine Brake Specific Fuel Consumption Contour

Chemical reaction inside cylinder during the combustion process is very difficult to model due to its transient and heterogeneous character, primarily controlled by the turbulent mixing of injected fuel and the fresh intake air [32]. So it is hard to predict the NO<sub>x</sub> and Soot emission. Researchers attempted to develop two-zone combustion model, multi-zone combustion models driven by the desire to predict accurate exhaust emissions. Hongusk Kim [33] investigated the effect of Exhaust Gas Recirculation on heavy-duty diesel engine performance and developed and modified KIVA-3V code to test the NO and Soot emissions. The multidimensional engine model was used in investigation. Pia Kilpinen [13] improved a sub-model for NO emission prediction for medium-speed, four-stroke, direct-injection marine engine and the trend of increasing NO emission with increasing load was correctly predicted.

Comparing with lower zones diesel combustion models, the advantage of multi-dimensional models is available for the detailed spatial information and interactions of phenomena. However, the accurate prediction results from multi zone models are based on the relative inadequacy of turbulence, combustion chemistry sub-models. And multi-dimensional models require longer computing time and storages capacity [9]. Therefore, in our case, the single-zone model is a reasonable choice for our control purpose.

EGR was considered as an effective means for reducing flame temperature and NO<sub>x</sub> emission [35]. The control inputs to the diesel engine include the fuel injection, injection time, boost and EGR, while the outputs are the in-cylinder pressure, in-cylinder temperature and heat release rate etcetera. Figure 2- 1 shows a flow chart of the diesel thermodynamic model and NO<sub>x</sub> and soot emission model. As mentioned before the thermodynamic model receives the input signals of fuel injection, injection timing, boost and EGR. From this, in-cylinder pressure, heat release rate and in-cylinder temperature can be calculated. The instantaneous in-cylinder pressure, temperature and heat release rate can be used as inputs of the emission estimation models.

After comparing the experimental data from Clean Diesel Engine Lab to the estimation results, the model was tuned in order to complete the model validation. In the following sections the detailed information about the diesel thermodynamic model and sub-models and the emission estimation model is shown.

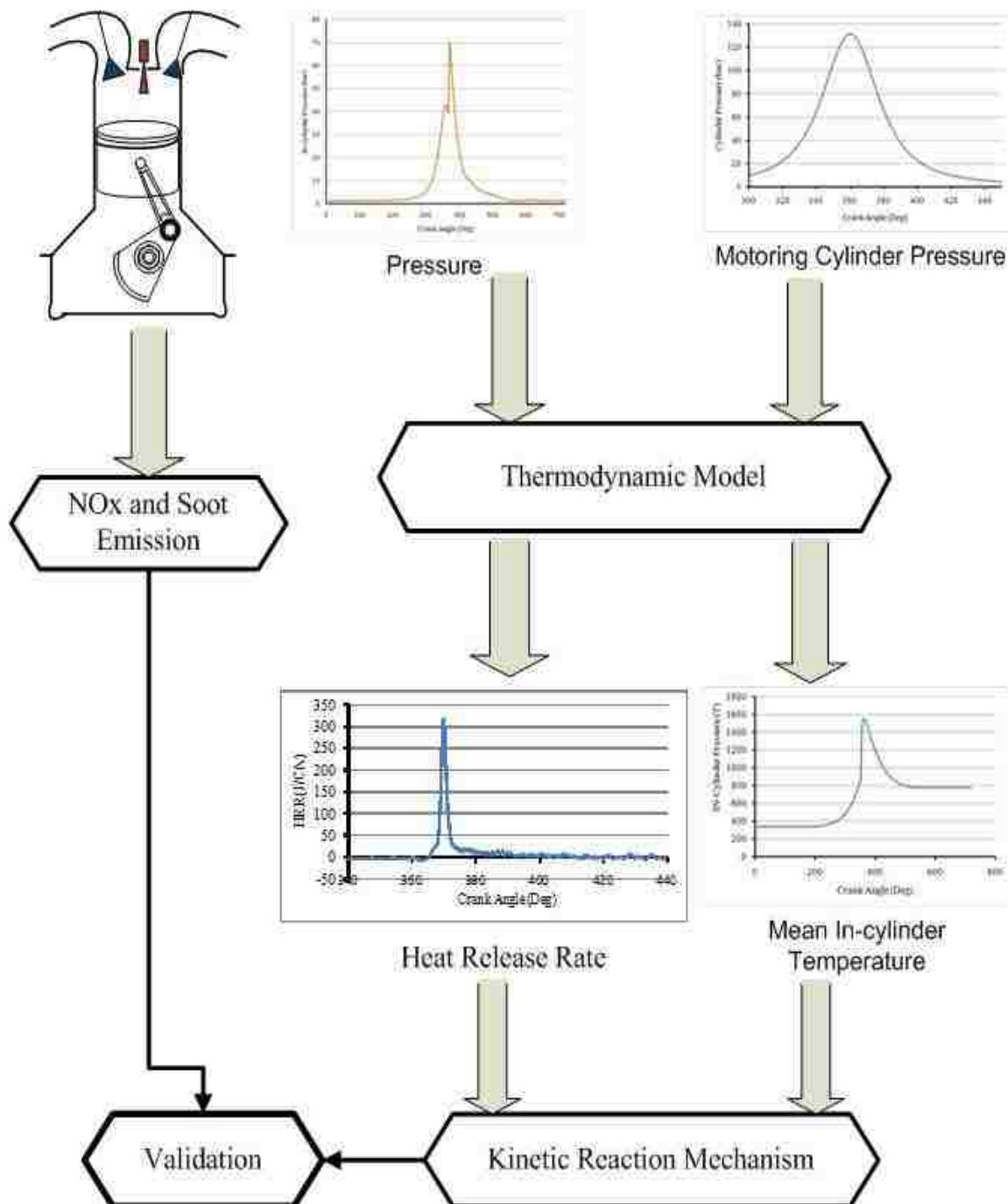


Figure 2- 2 Thermodynamic Engine Model and Emission Estimation Model

## 2.1 Combustion Model

According to the first law of the thermodynamics, the change of the internal energy of a system

during a process is the sum of the changes in its heat transfer and work transfer. Figure 2- 3 indicates the thermodynamic engine model. The first law of thermodynamics is implemented with the ideal -gas equation of state [34].

$$dQ = dE + pdV \quad (2.1)$$

$$[OH] = 2.129 \times 10^2 \times T^{(-0.57)} \times e^{(-4595/T)} \times [O]^{0.05} \times [H_2O]^{1/2} \quad (2.2)$$

Where:  $R$  is the universal gas constant ( $R=8.31447 \text{ kJ/kmol} \cdot K$ );

$P$  (pa) is the absolute pressure;

$T$  (K) is the absolute temperature;

$V$  ( $m^3$ ) is the instantaneous cylinder volume;

The instantaneous cylinder volume consists of a clearance volume  $V_c$  and the instantaneous displacement volume. The instantaneous displacement volume is a function of crank angle, cylinder bore, crank radius, compression ratio and the length of connecting rod.

$$r_c = \frac{\text{Maximum Cylinder Volume}}{\text{Minimum Cylinder Volume}} = \frac{V_d + V_c}{V_c} \quad (2.3)$$

$$V = \frac{\pi D^2}{4} \left\{ \frac{S}{r_c - 1} + \frac{S}{2} \left[ \left( 1 + \frac{1}{R} \right) - \cos\left(\frac{\pi}{180} \theta\right) - \frac{1}{R} \sqrt{1 - R^2 \sin^2\left(\frac{\pi}{180} \theta\right)} \right] \right\} \quad (2.4)$$

Where  $V_c$  is the clearance volume;

$V_d$  is the displaced volume;

$r_c$  is the compression ratio;

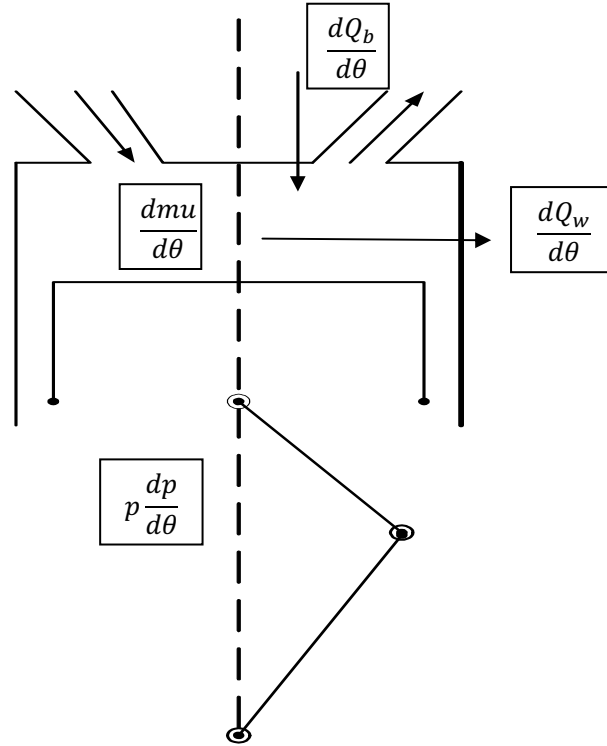


Figure 2- 3 Thermodynamic Engine Model

For the air surrounding the injected fuel, the first law of thermodynamic can be written as following equation:

$$\frac{dU}{d\theta} = p \frac{dV}{d\theta} - \frac{dQ_b}{d\theta} - \frac{dQ_w}{d\theta} \quad (2.5)$$

$$(M_{air} + X_{(i)} \times M_{fuel}) C_p (T_{(i)} - T_{(i-1)}) = LHV \times M_v \times (\theta_{(i)} - \theta_{(i-1)}) - p_{(i-1)} (V_{(i)} - V_{(i-1)}) - Q_{w(i)} \quad (2.6)$$

The equation for the mean mixture temperature is derived as follows:

$$T_{(i)} = T_{(i-1)} + \frac{LHV \times M_v \times (\theta_{(i)} - \theta_{(i-1)}) - p_{(i-1)} (V_{(i)} - V_{(i-1)}) - Q_{w(i)}}{M_{air} + X_{(i)} \times M_{fuel}} \quad (2.7)$$

Where:  $LHV$  is the lower heating value; (Assuming  $LHV=42.5$  MJ/kg)

$M_{fuel}$  (kg) is the injected fuel;

$C_p$  is the specific heat capacity;

$M_{air}$  (kg) is the mass of in-cylinder air;

$M_v$ (kg) is the evaporated fuel at each step size;

$Q_w$  is the heat transfer from cylinder wall, cylinder head and piston;

$X$  is the burn fraction of the injected fuel;

$T$  is the in-cylinder temperature;

The compression process is assumed as a polytropic compression process;

$$P_0 V_0^\gamma = P V^\gamma \quad (2.8)$$

Where:  $P_0$  (pa) is the in-cylinder pressure when the crank angle starts from  $180^\circ$ ;

$V_0$  ( $m^3$ ) is the in-cylinder volume when the crank angle starts from  $180^\circ$ ;

$P$  (pa) is the in-cylinder pressure when the crank angle is after  $180^\circ$ ;

$V$  ( $m^3$ ) is the in-cylinder volume when the crank angle is after  $180^\circ$ ;

The equations for the in-cylinder pressure and in-cylinder temperature are as follows during the compression process.

$$P_{(i+1)} = P_{(i)} \left( \frac{V_{(i)}}{V_{(i+1)}} \right)^\gamma \quad (2.9)$$

$$T_{(i+1)} = \frac{P_{(i+1)} V_{(i+1)}}{P_{(i)} V_{(i)}} T_{(i)} \quad (2.10)$$

## 2.2 Heat Release Model

The in-cylinder combustion is a very complex process, and the extensive modeling would be helpful. The analytical functions computing the burn rate is used in this thesis. The prevailing of these functions is the Wiebe function, which can be used to predict the burn fraction and burn rate for different engine systems [43][44].

Equation (2.11) and (2.12) are used to calculate the mass burning fraction and absolute value of heat release [42].

$$X_b = (1 - \alpha_{wall}) \left\{ 1 - \exp\left(-a \left(\frac{\theta - \theta_0}{\Delta\theta}\right)^{m+1}\right) \right\} + \alpha_{wall} \left\{ 1 - \exp\left(-a \left(\frac{\theta - \theta_0}{K_{wall} \Delta\theta}\right)^{m+1}\right) \right\} \quad (2.11)$$

$$\frac{dQ_B}{d\theta} = M_{fuel} \times LHV \times \frac{dX_b}{d\theta} \quad (2.12)$$

Where :  $X_b$  is the mass fraction burned;

$\theta$  is the crank angle;

$\theta_0$  is the crank angle when the combustion starts (SOC);

$\Delta\theta$  is the total combustion duration;

$M$  is the adjustable parameter;

$A$  is the adjustable constant relating to the combustion duration;

$\alpha_{wall}$  is the fraction of the mixture that burns in the slow combustion region;

$K_{wall}$  is the ratio of slow burn duration to the standard burn duration;

$$a = a_{10-90} = \left( \left( \ln\left(\frac{1}{1-0.9}\right) \right)^{1/(m+1)} - \left( \ln\left(\frac{1}{1-0.1}\right) \right)^{1/(m+1)} \right)^{m+1} \quad (2.13)$$

For diesel engines, the in-cylinder pressure, temperature and swirl ratio directly affect the ignition delay (ID). Many corrections have been made to predict the ignition delay for diesel engines [45][46]. The most widely accepted correlation was given by an Arrhenius expression [45], which is a function of ambient gas pressure and temperature.

$$ID = Fp^{-N} \exp\left(\frac{E}{R_u T}\right) \quad (2.14)$$

Where:  $p$  and  $T$  are the cylinder pressure and temperature,  $E$  is the activation energy,  $R_u$  is the universal gas constant,  $N$  and  $F$  are experimental constants.

For diesel fuel, Wolfer (1950) [23] achieved a reasonable estimate from the following equation.

$$ID = 3.45 \exp\left(\frac{2100}{T}\right) p^{-1.02} \quad (2.15)$$

### 2.3 Heat Transfer Model

Convective mode of heat transfer contributes to 80% of the total engine heat transfer [9]. For typical diesel engines, the heat transfer process starts from the in-cylinder mixture within the cylinder via the combustion chamber wall to the coolant. Both the convective heat transfer and radiation heat transfer contribute to the heat flux through the wall. Based on the experiment results, Annand [9] developed the convective heat-transfer correlation for cylinder head. In this thesis, Woschni's approach is used.

$$\frac{dQ_w}{d\theta} = \sum_{i=1}^3 \frac{dQ_w}{d\theta} = \frac{1}{w} \times \sum_{i=1}^3 h_c \times A_i \times (T - T_w) \quad (2.16)$$

Where:  $T$  is the in-cylinder temperature (k).

$T_w$  is the temperature of cylinder wall, cylinder head and piston head.

$h_c$  is the coefficient of convective heat transfer;

$i=1$ : Cylinder head;  $i=2$ : Piston;  $i=3$ : Cylinder wall;

$A$  is the heat transfer area ( $m^2$ );

According to Woschni's correlation, the equation for the coefficient of heat transfer is summarized as:

$$h_c = 3.26 \times D^{-0.2} \times p^{0.8} \times T^{-0.55} \times w^{0.8} \quad (2.17)$$

Where:  $D$  is the cylinder bore (m);

$p$  is the in-cylinder pressure (kPa);

$T$  is the cylinder temperature (K);



$W$  is the average cylinder gas velocity (m/s);

The average cylinder gas velocity for a four stroke, direct injection compression ignition engine was expressed as follows:

$$w = C_1 S_p + C_2 \frac{V_d T_r}{P_r V_r} (p - p_m) \quad (2.18)$$

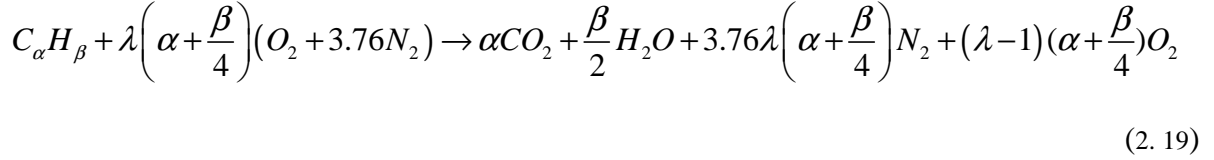
Where:  $V_d$  is the displaced volume;  $p$  is the instantaneous in-cylinder pressure;  $P_r, T_r, V_r$  are the in-cylinder pressure, temperature and volume when the crank angle is  $180^\circ$ ;  $p_m$  is the motored cylinder pressure at the same crank angle as  $p$ ;  $C_1 = 2.28$ ;  $C_2 = 3.24 \times 10^{-3}$ ;

## 2.4 EGR System

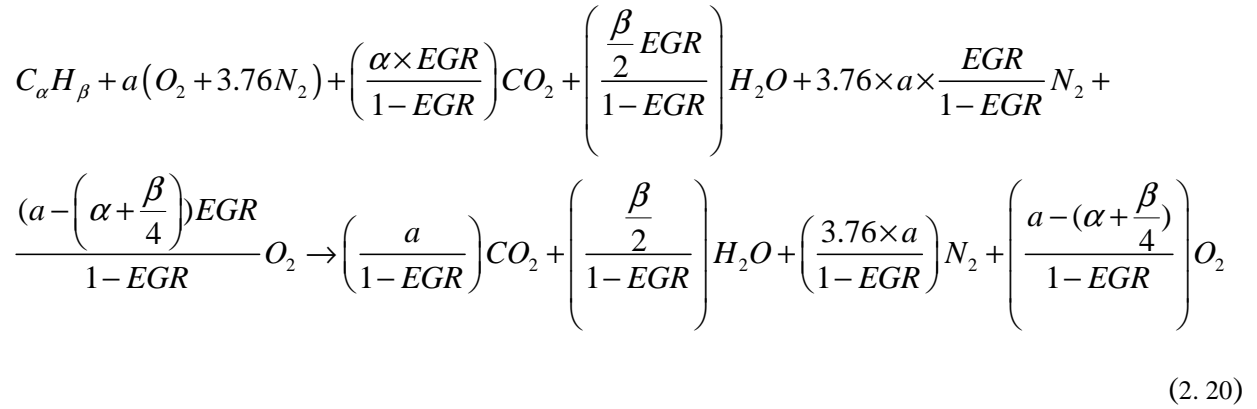
EGR systems work by recirculating different amounts of an engine's exhaust gas back to the engine cylinder. Combining the exhaust gas recirculation technology is recognized as the only possible way to achieve future emission restriction target by internal measures [54]. EGR is defined as the ratio of intake manifold  $\text{CO}_2$  concentration to exhaust manifold  $\text{CO}_2$  concentration [53]. EGR system interferes with the diesel combustion system through thermal, chemical and dilution effects. When an EGR system is incorporated into the diesel engine, the amount of  $\text{NO}_x$  emissions are reduced due to lower in-cylinder temperatures during the combustion process. The application of EGR is regarded as one of the essential means of reducing oxides of nitrogen ( $\text{NO}_x$ ) emission from diesel engines. However, for intermediate and low engine loads, EGR increases the particulate emissions and specific fuel consumption [36]. Equation (2.19) describes the complete combustion process without EGR while the equation (2.20) describes the combustion process when diesel engine incorporates EGR system. In the diesel engine model calculations for this work, the second equation was used. In order to validate the simulation results, the calculation was conducted by using a typical diesel fuel formulation. Ultimately, the

formula  $C_1H_{1.7}$  was used in the simulation.

The complete combustion equation (without EGR) when  $\lambda > 1$



The complete combustion equation (with EGR)



Where  $EGR = \frac{N_{CO_2, intake}}{N_{CO_2, exhaust}}$   $a = \lambda \times \left( \alpha + \frac{\beta}{4} \right)$

The mass fraction of the  $CO_2$  from exhaust:

$$MASS\_CON\_CO_2 = \frac{\frac{\alpha \times EGR}{1 - EGR} \times 44}{\frac{\alpha \times EGR}{1 - EGR} \times 44 + \frac{\frac{\beta}{2} EGR}{1 - EGR} \times 18 + 3.76 \times a \times \frac{EGR}{1 - EGR} \times 28 + \frac{(a - \left( \alpha + \frac{\beta}{4} \right)) EGR}{1 - EGR} \times 32} \quad (2.21)$$

Where:  $a = \alpha + \frac{\beta}{4}$

Amount of  $O_2$  (mole) consumed each step size (0.1 Crank Angle):

$$n\_rac\_O_2 = n\_fuel \times \left( \alpha + \frac{\beta}{4} \right) \quad (2.22)$$

Where:  $n_{fuel}$  is the amount of fuel consumed each step size (0.1 Crank Angle);

Amount of CO<sub>2</sub>, H<sub>2</sub>O produced each step size (0.1 Crank Angle):

$$n_{rac\_CO_2} = n_{fuel} \times \left( \frac{a}{1-EGR} - \frac{\alpha \times EGR}{1-EGR} \right) \quad (2.23)$$

$$n_{rac\_H_2O} = n_{fuel} \times \left( \frac{\frac{\beta}{2}}{1-EGR} - \frac{\frac{\beta}{2} EGR}{1-EGR} \right) \quad (2.24)$$

$$n_{O_2}(i) = n_{O_2}(i-1) + n_{rac\_O_2} \quad (2.25)$$

$$n_{CO_2}(i) = n_{CO_2}(i-1) + n_{rac\_CO_2} \quad (2.26)$$

$$n_{H_2O}(i) = n_{H_2O}(i-1) + n_{rac\_H_2O} \quad (2.27)$$

$$n_{total}(i) = n_{CO_2}(i) + n_{H_2O}(i) + n_{O_2}(i) + n_{N_2}(i) \quad (2.28)$$

The mole fraction of O<sub>2</sub>, N<sub>2</sub>, CO<sub>2</sub>, H<sub>2</sub>O are as follows:

$$O_2\_mole\_frac(i) = \frac{n_{O_2}(i)}{n_{total}(i)} \quad (2.29)$$

$$N_2\_mole\_frac(i) = \frac{n_{N_2}(i)}{n_{total}(i)} \quad (2.30)$$

$$CO_2\_mole\_frac(i) = \frac{n_{CO_2}(i)}{n_{total}(i)} \quad (2.31)$$

$$H_2O\_mole\_frac(i) = \frac{n_{H_2O}(i)}{n_{total}(i)} \quad (2.32)$$

## CHAPTER 3 CONTROL ORIENTED NO<sub>x</sub> AND SOOT ESTIMATION

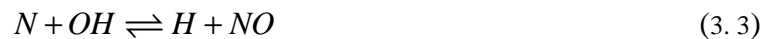
### 3.1 NO<sub>x</sub> Emission Estimation

In-cylinder NO<sub>x</sub> formation occurs from three fundamentally different reactions. In year 1946, Zeldovich [9] was the first to suggest the importance of reactions equation (3.1) and (3.2). For internal combustion engine, the primary source is the thermal NO forming from the thermal dissociation equation (3.1) and the subsequent reaction of nitrogen and oxygen molecules from the combustion air [10].

The governing equations for the thermal NO<sub>x</sub> from molecular nitrogen are as follows:



The mechanism of NO formation from Zeldovich has been well accepted and understood extensively. Later on, Lavoie [9] added the reaction (3.3) to the Zeldovich Mechanism and contributed significantly to the study. Due to the temperature sensitivity, the mechanism including equation (3.1), (3.2) and (3.3) is referred to as the thermal mechanism.



Applying the chemical kinetic rate law for the equations presented above, the formation rate of NO is given by:

$$\frac{d[NO]}{dt} = k_{f,1}[O][N_2] + k_{f,2}[N][O_2] + k_{f,3}[N][OH] - k_{r,1}[NO][N] - k_{r,2}[NO][O] - k_{r,3}[NO][H]$$

(3.4)

Note: All concentrations have a unit of mol/m<sup>3</sup>

The rate constants measured from experimental studies have been evaluated by Hanson and Salimian[49]and the expressions are shown below.

$$k_{f,1} = 1.8 \times 10^8 e^{-38370/T} \quad (3.5)$$

$$k_{f,2} = 1.8 \times 10^4 T e^{-4680/T} \quad (3.6)$$

$$k_{f,3} = 7.1 \times 10^7 e^{-450/T} \quad (3.7)$$

$$k_{r,1} = 3.8 \times 10^7 e^{-425/T} \quad (3.8)$$

$$k_{r,2} = 3.81 \times 10^3 T e^{-20820/T} \quad (3.9)$$

$$k_{r,3} = 1.7 \times 10^8 e^{-24560/T} \quad (3.10)$$

Where  $k_{f,1}$ ,  $k_{f,2}$ ,  $k_{f,3}$  are the rate constants for the forward reactions.  $k_{r,1}$ ,  $k_{r,2}$ ,  $k_{r,3}$  are the rate constants for the corresponding reverse rate constants.

According to Westenberg[50], the equilibrium O-atom concentration can be derived as follows:

$$[O] = k_p \times [O_2]^{1/2} \quad (3.11)$$

$$[O] = 36.64 \times T^{-1/2} \times [O_2]^{1/2} \times e^{-27123/T} \quad (3.12)$$

The partial equilibrium approach was chosen to determine the OH radical concentration.

$$[OH] = 2.129 \times 10^2 \times T^{-0.57} \times e^{-4595/T} \times [O]^{1/2} \times [H_2O]^{1/2} \quad (3.13)$$

Finally, the expression for the rate of change NO concentration is shown as follows

$$\frac{d[NO]}{dt} = 2k_{f,1}[O][N_2] \left( \frac{1 - \frac{k_{r,1}k_{r,2}[NO]^2}{k_{f,1}[N_2]k_{f,2}[O_2]}}{1 + \frac{k_{f,1}[NO]}{k_{f,2}[O_2] + k_{f,3}[OH]}} \right) \quad (3.14)$$

As mentioned previously, the rate of formation of NO is significant at high temperatures, which results from the large amount of energy required to break the strong N<sub>2</sub> triple bond. This effect is illustrated by the high activation energy of reaction equation (3.1). Since the activation energy for nitrogen-atom oxidation is small, with sufficient oxygen provided, the free nitrogen atoms consumption rate equals to its formation rate and therefore a quasi-steady state can be achieved [50]. Except for extremely fuel-rich combustion conditions, this assumption can be applied for most combustion cases. The indicated forward and reverse reaction rates introduce the uncertainty to the prediction with actual in-cylinder pressure and temperature.

### 3.2 Soot Emission Estimation

The most popular semi-empirical model is the two-step Hiroyasu model [51]. According to his model, the soot formation process considered involves two reaction steps: the formation step and the oxidation step. When the formation reaction begins, at the same time, the oxidation step is carried on. Therefore the amount of soot produced is equal to the soot production of the formation reaction minus the oxidation reaction. In the formation step, shown in equation (3.16), soot is directly related to fuel vapor molecules whereas during the oxidation step, shown in the equation (3.17), soot particles decrease due to the presence of molecular oxygen. The pressure of O<sub>2</sub> can be derived from the engine combustion model.

Soot formation rate equals to the amount of formed soot minus the oxidized soot [37].

$$\frac{dm_{soot}}{dt} = \left( \frac{dm_{soot}}{dt} \right)_{form} - \left( \frac{dm_{soot}}{dt} \right)_{oxid} \quad (3.15)$$

$$\frac{dm_{soot\_form}}{dt} = A_1 \times \exp\left(-\frac{T_{A1}}{T}\right) \times M_{fuel\_v} \times \left(\frac{p_{gas}}{p_{gas\_ref}}\right)^{n1} \quad (3.16)$$

$$\frac{dm_{soot\_oxid}}{dt} = A_2 \times \exp\left(-\frac{T_{A2}}{T}\right) \times (m_{soot})^{n2} \times \left(\frac{p_{O_2}}{p_{O_2\_ref}}\right)^{n3} \quad (3.17)$$

Where:  $A_1$  is the constant for soot formation;

$A_2$  is the constant for soot oxidation;

$T_{A1}$  is the activation temperature for soot formation reaction [6313K];

$T_{A2}$  is the activation temperature for soot oxidation reaction [7070K];

$M_{fuel\_v}$  is the currently vapor fuel mass (kg);

$p_{gas}$  is the in-cylinder pressure (bar);

$p_{gas\_ref}$  is the gas reference pressure (bar);

$p_{O_2}$  is the partial pressure of  $O_2$  (bar);

$p_{O_2\_ref}$  is the  $O_2$  reference partial pressure (bar);

$$n_1 = 1.8; n_2 = 1.0; n_3 = 1.0;$$

Due to its simplicity, this model has been widely utilized [37][38][39]. It can be incorporated into the single-zone, two-zone and multi-zone engine combustion models [40][26].

In order to calculate the soot formation rate, in-cylinder current vapor fuel mass is required. C.O. Schmalzing [41] proposed a holistic injection model to optimize fuel injection in the Diesel engine system. Comparing to measured liquid and vapor phase penetration lengths for different operating conditions, the calculated results were validated. According to the simulation results

from [41], the relation of vaporizing percentage and crank angle was generated and utilized for the current vapor fuel mass calculation, which is shown in Figure 3- 1.

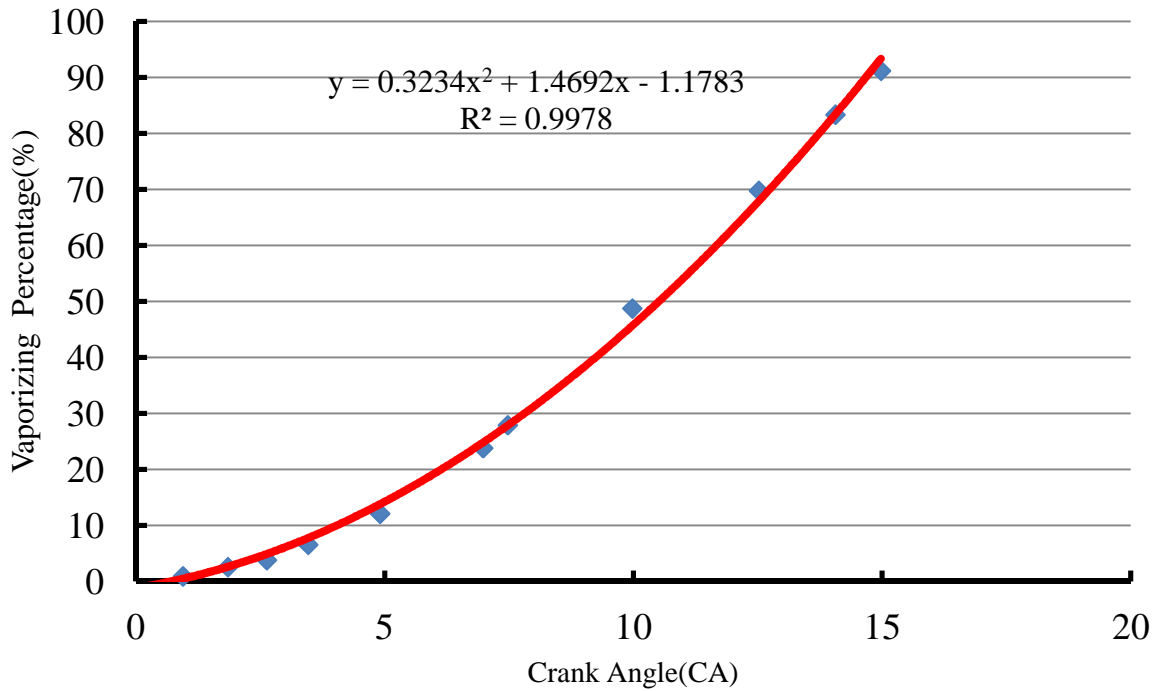


Figure 3- 1 Vaporizing Percentage VS. Crank Angle (Injection Pressure  $P_{inj}=80$  MPa)



## CHAPTER 4 EXPERIMENT SETUP AND ESTIMATION

### RESULT VALIDATION

#### 4.1 Experiment Setup

The experimental investigation was conducted on a single cylinder, four-stroke, common rail diesel engine of 0.76 lit displacement volume. The experiment engine bench setup and engine geometrical specifications are shown in Figure 4- 1 and Table 4- 1.

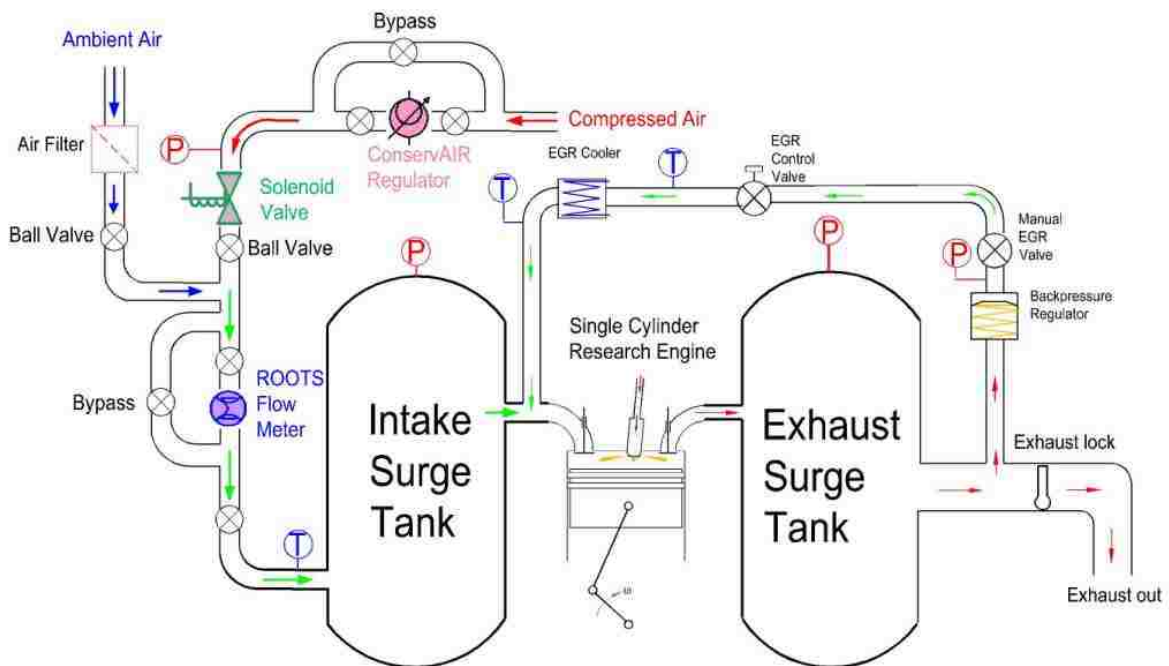


Figure 4- 1 Single Cylinder Research Engine Test Platform

The experimental investigations in this thesis have been carried out under independently controlled levels of engine boost, exhaust backpressure and EGR valve opening. In order to

measure the in-cylinder pressure to obtain combustion information, an AVL G13P pressure piezoelectric transducer was mounted and connected through a Kistler 5010B charge amplifier. Based on the computer code developed in Labview control software, the control of high speed acquisition system had been achieved. A dual-bank exhaust analyzer system (for NO<sub>x</sub>, HC, CO<sub>2</sub> and O<sub>2</sub>) has been installed for the exhaust emissions and intake gas concentration for exhaust analysis. A CAI 6000 Series chemiluminescence detector and an AVL smoke meter are used to measure NO<sub>x</sub> and Filter Smoke Number. The following equation was used to convert FSN to soot mass concentration in the unit of [mg/m<sup>3</sup>].

$$Soot \left[ mg / m^3 \right] = 1.8419 \times [FSN]^3 + 2.9545 \times [FSN]^2 + 12.815 \times [FSN] - 0.0305 \quad (4.1)$$

## 4.2 Estimation Result Validation

In order to affect the comparison results, it was necessary to carry out the parametric analysis of the sub-model constants to tune the model.

- 1) Determining the values for adjustable constants of Weibe heat release model in order to make sure that the calculated in-cylinder pressures match the experimental pressures measured from the cylinder pressure transducer. When  $m$  value equals to 1, the in-cylinder pressure and heat release rate curve match with the empirical results with  $k_{wall} = 0.34$  and  $\alpha = 0.36$ . The temperature of the cylinder walls was chosen equal to 500K.
- 2) Determining the values for the reaction constants of the NO<sub>x</sub> formation so that the calculated results of NO<sub>x</sub> formation will match the experimental values. According to the NO<sub>x</sub> estimation mechanism, the rate constants for the forward reactions and corresponding reverse rate constants were set as follows:

$$k_{f,1} = 2.8 \times 10^8 e^{-42000/T} \quad (4.2)$$

$$k_{f,2} = 1.8 \times 10^4 T e^{-4680/T} \quad (4.3)$$

$$k_{f,3} = 7.1 \times 10^7 e^{-450/T} \quad (4.4)$$

$$k_{r,1} = 3.8 \times 10^7 e^{-425/T} \quad (4.5)$$

$$k_{r,2} = 3.81 \times 10^3 T e^{-20820/T} \quad (4.6)$$

$$k_{r,3} = 1.7 \times 10^8 e^{-24560/T} \quad (4.7)$$

The constants for the equilibrium O-atom and OH radical concentration were chosen as follows:

$$[O] = 36.64 \times T^{1.24} \times [O_2]^{1.4} \times e^{-28400/T} \quad (4.8)$$

The partial equilibrium approach was chosen to determine the OH radical concentration.

$$[OH] = 2.129 \times 10^2 \times T^{(-0.57)} \times e^{(-4595/T)} \times [O]^{0.05} \times [H_2O]^{1/2} \quad (4.9)$$

- 3) Determining the values for the reaction constants of the soot formation so that the soot formation will match the experimental values. For soot estimation mechanism, the constants for soot formation and oxidation were set as  $A_1 = 1.6 \times 10^{-4}$  and  $A_2 = 3200$ . And the exponent of pressure in the soot formation and oxidation equations  $n_1=3$  and  $n_3=0.9$  are chosen to fit the experimental results. The activation temperatures are found in [37],  $T_{A1}=3200k$  and  $T_{A2}=7070k$ .

Before utilizing the thermodynamic model and emission estimation for the 8 operating points, it is necessary to validate their ability to provide the engine performance information and emission profile. In this chapter, the calculated and measured results of in-cylinder pressure, temperature, cumulative heat release, NO formation concentration and soot formation concentration as a function of crank angle will be presented. The measured experimental data and calculated results

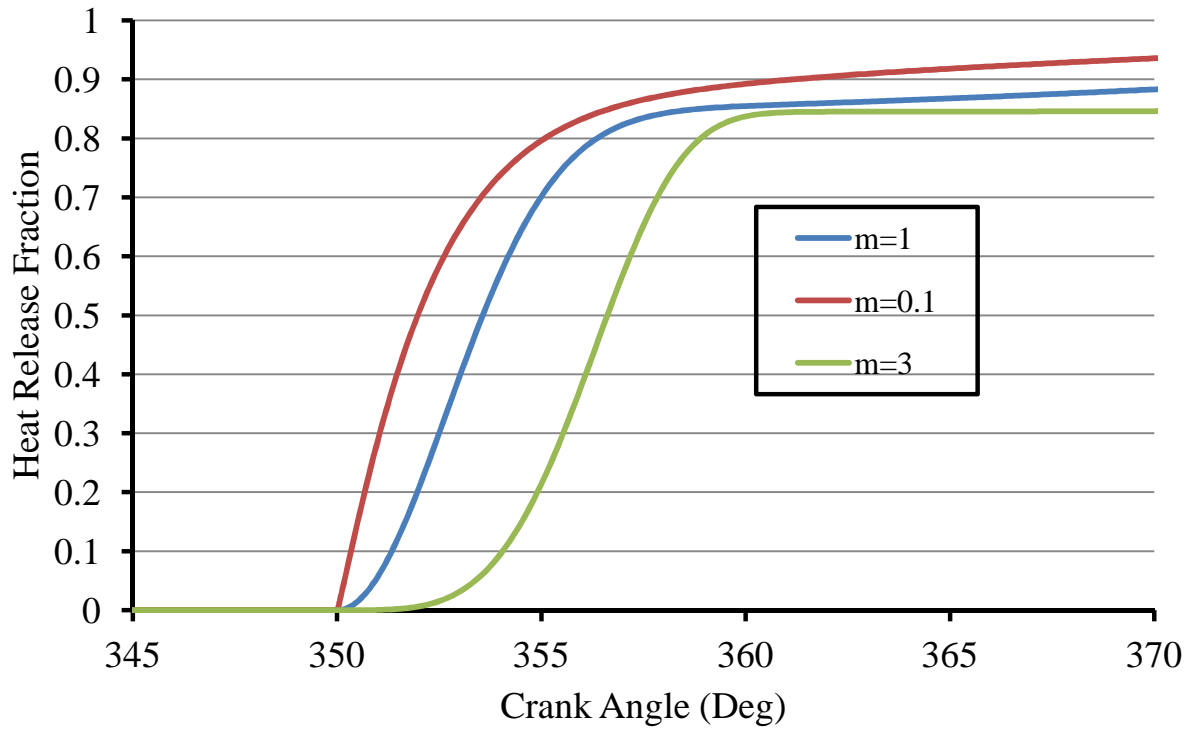
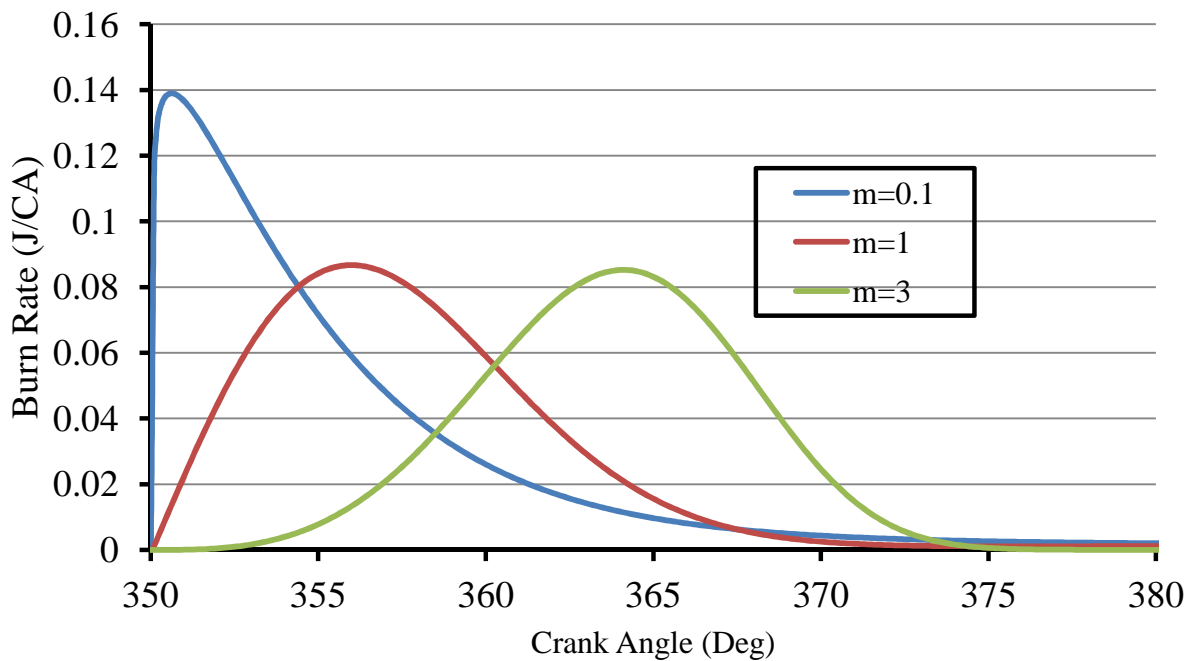
are depicted in the following figures in a comparative way. Table 4-1 presents the specification of single cylinder research engine used for the engine performance and emission estimation validation.

Table 4- 1 Single Cylinder Research Engine Geometrical Specification

| SINGLE CYLINDER I-TEC ENGINE SPECIFICATIONS |                     |
|---|---------------------|
| Bore (mm)                                   | 96                  |
| Stroke (mm)                                 | 105                 |
| Connecting Rod (mm)                         | 176                 |
| Compression Ratio                           | 14.3                |
| Combustion System                           | Direction Injection |
| Injection System                            | Common rail         |

The experimental data shown here was collected from the Clean Diesel Engine Laboratory (University of Windsor). The operating conditions for the EGR Sweep are as follows: Engine speed = 1200 rpm, IMEP = 8 bar, Boost = 1.4 bar, Injection pressure = 1200 bar and CA 50 = 368 CA. The range of the EGR sweep is from 8% to 43% depending on the engine operating condition examined.

The detailed information of governing equations for heat release rate calculation was presented in Chapter 2. Figure 4-2 illustrates the heat release fraction with different  $m$  values between 0.1 and 3 for the combustion duration of 8 crank angle degrees. With higher  $m$  value, the combustion is retarded. The burning rate is shown in Figure 4-3 when the combustion duration was fixed at 40 crank angle degrees with different  $m$  values.

Figure 4- 2 Heat release rate with different  $m$  valueFigure 4- 3 Burn rates for constant combustion duration and different values of  $m$

In the internal combustion engine analysis, the in-cylinder pressure has been considered to be an important experimental diagnostic in the development of automotive engine research [43]. The in-cylinder pressure profiles directly reflect the effects of in-cylinder heat release, heat transfer to the cylinder wall and head surface and work transfer. Figure 4- 4 and 4-7 present the predicted and measured in-cylinder pressure traces diagram when the EGR is 21% and 34% at speed of 1200 rpm. The computation time interval is 0.1 CA. It can be seen from the figure that the experimental data and simulation results appear to agree well with one another. After the first step of the analysis, it was verified that the model can effectively predict the in-cylinder pressure.

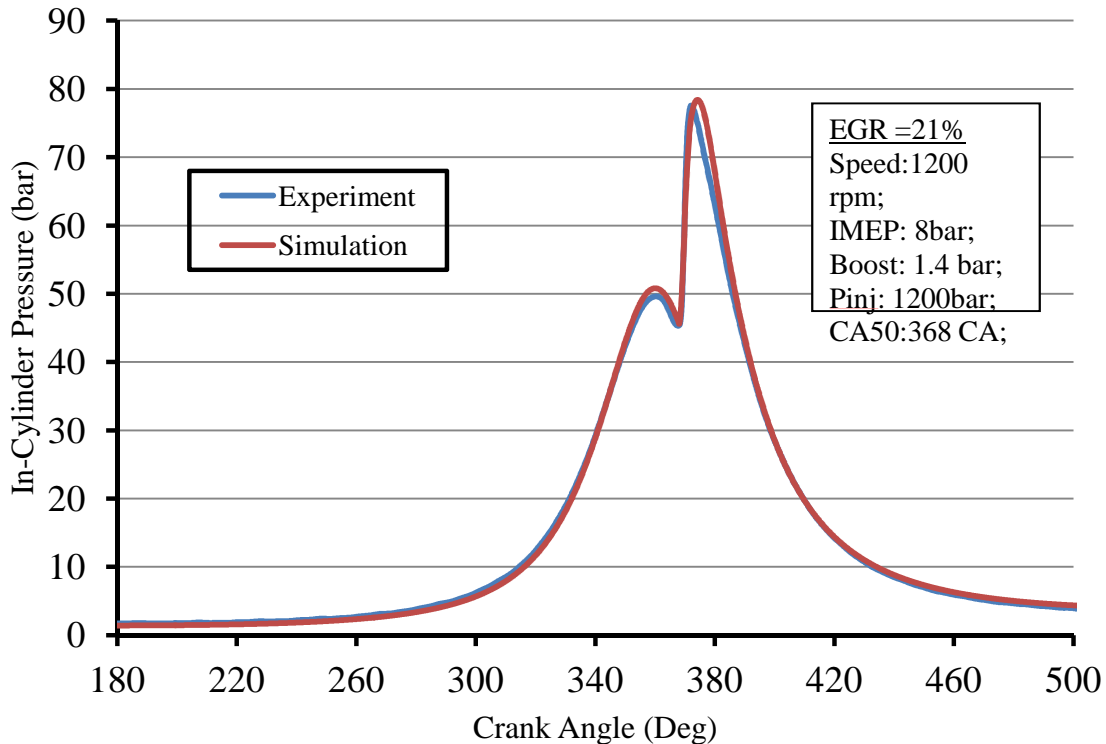


Figure 4- 4 Comparison of the calculated and experimental in-cylinder pressure (EGR=21%)

The good coincidence between the measured and calculated in-cylinder pressure was also achieved in other different EGR operating conditions. Appendix A shows the detail information about the comparisons.

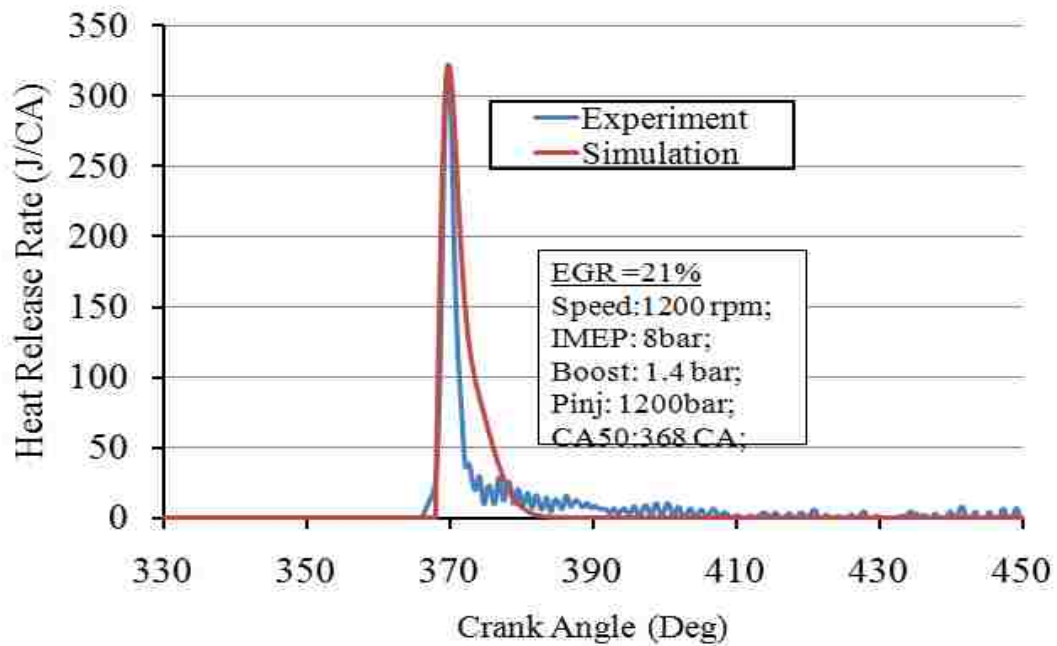


Figure 4- 5 Comparison of heat release rate from experiment and simulation (EGR=21%)

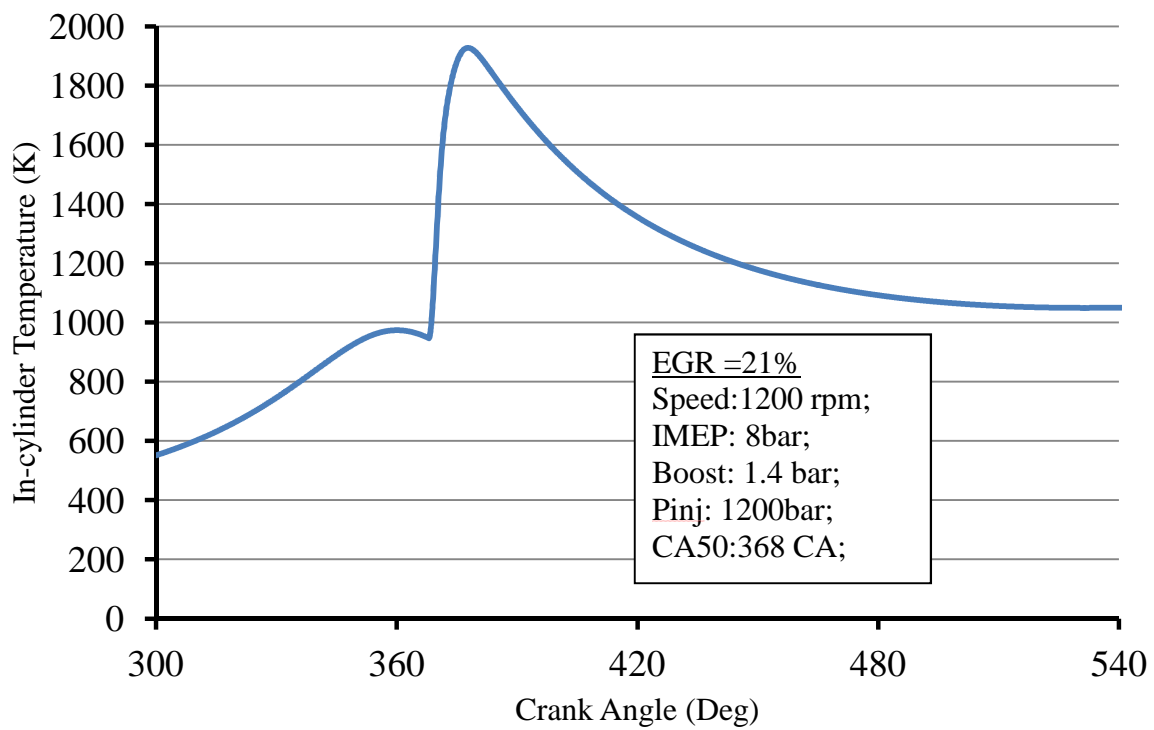


Figure 4- 6 Average in-cylinder temperature (EGR=21%)



The Figure 4-7 and Figure 4-8 illustrate the comparison of the computed and empirical results of the in-cylinder pressure and heat release rate when EGR equals to 34%. And they both follow the same trend as when EGR is 21%. Comparing the temperature results shown in Figure 4-6 (when EGR=21%), the mean cylinder temperature (shown in Figure 4-9) decreases due to the increase of EGR rate.

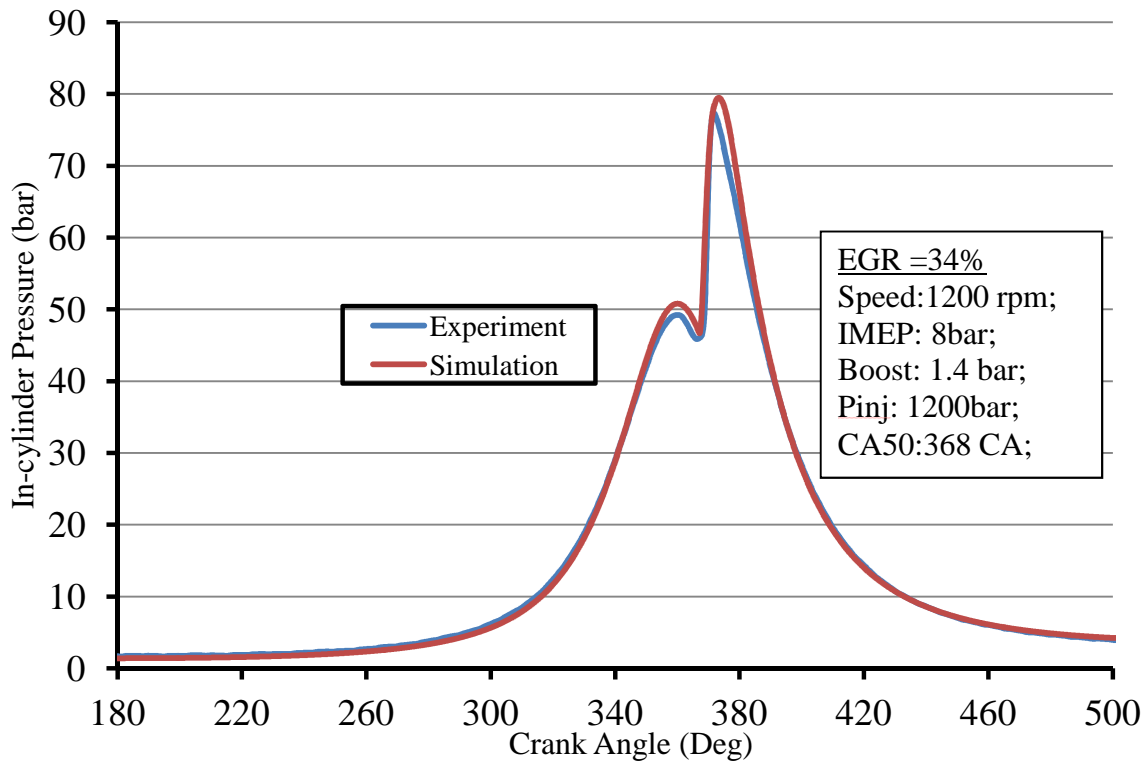


Figure 4- 7 Comparison of the calculated and measured in-cylinder pressure (EGR=34%)

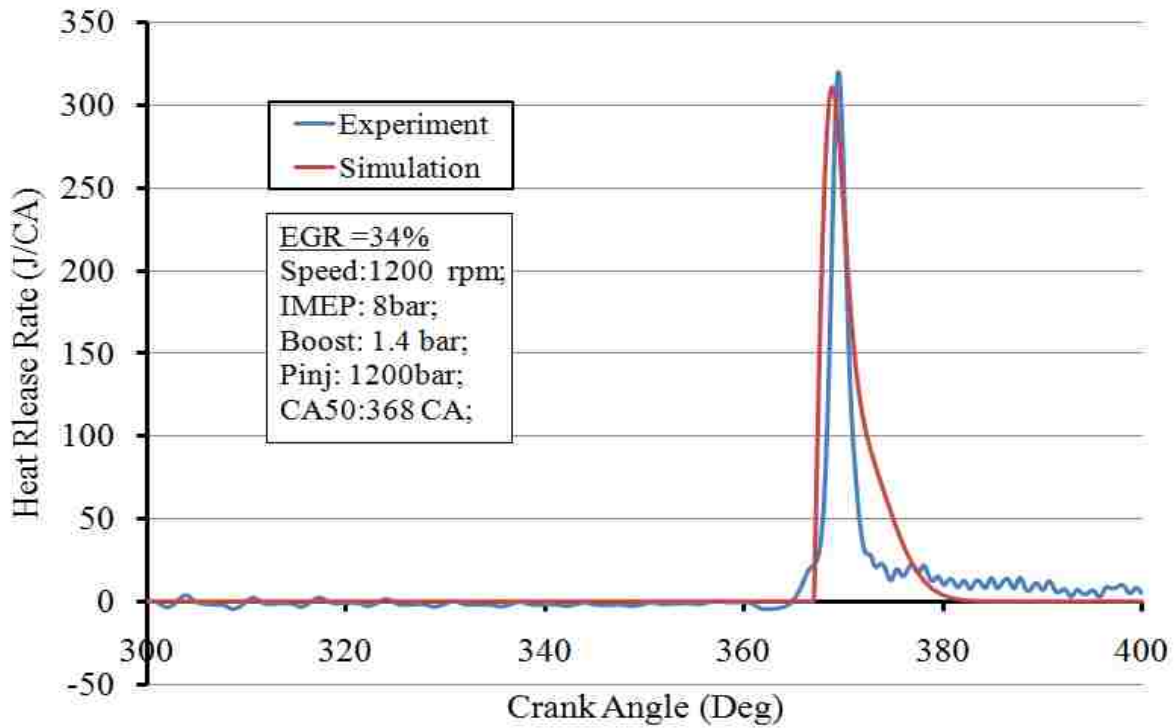


Figure 4- 8 Comparison of heat release rate from experiment and simulation (EGR=34%)

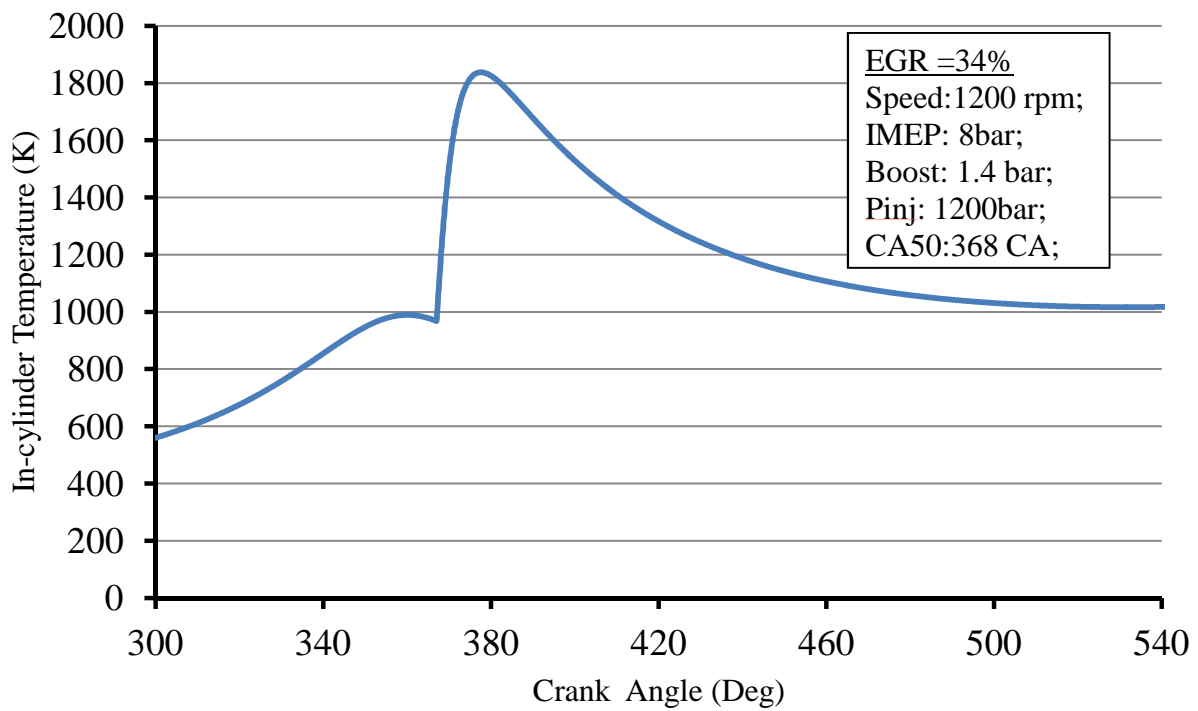


Figure 4- 9 Average in-cylinder temperature (EGR=34%)

Figure 4-10 and Figure 4-11 show the species mole fraction of O<sub>2</sub>, CO<sub>2</sub> and H<sub>2</sub>O during the combustion process with EGR=21% and EGR=34%.

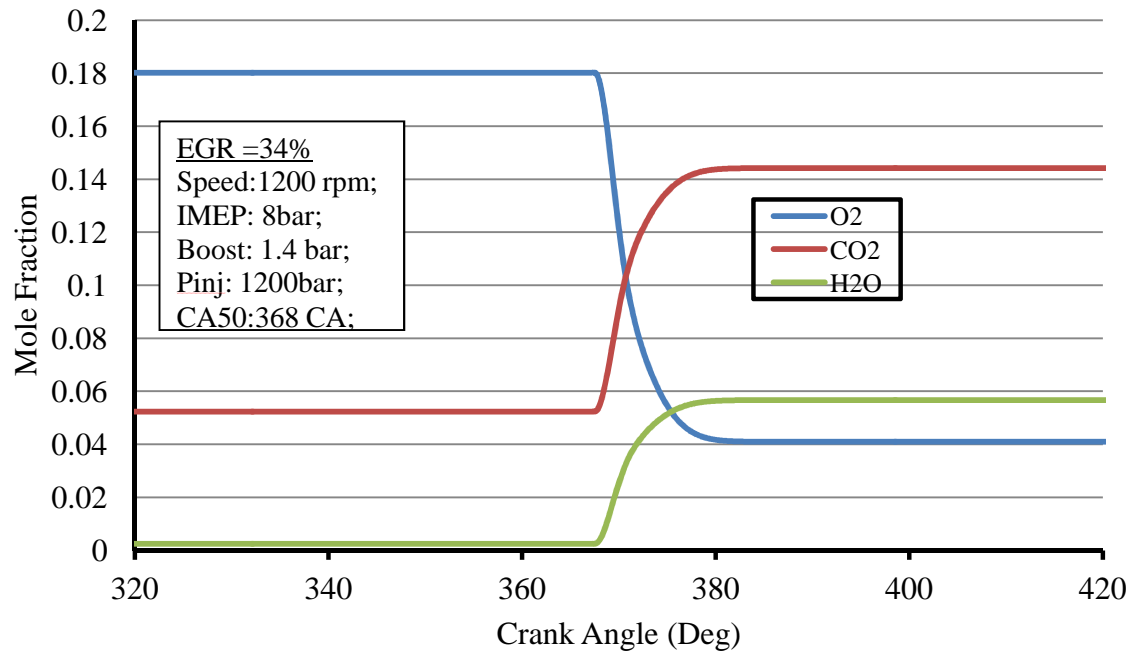


Figure 4- 10 Species (O<sub>2</sub> , CO<sub>2</sub> and H<sub>2</sub>O) mole fraction (EGR=34%)

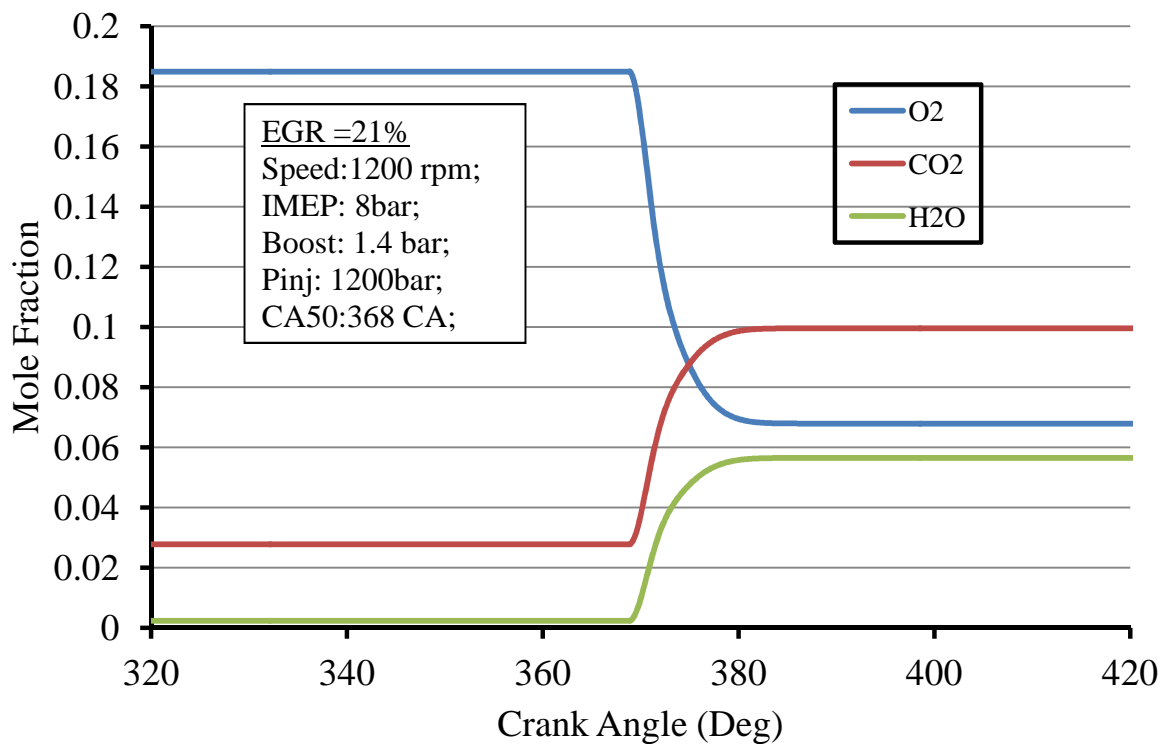


Figure 4- 11 Species (O<sub>2</sub>, CO<sub>2</sub>, and H<sub>2</sub>O) mole fraction (EGR=21%)

Figure 4- 12 shows the comparison of the calculated nitric oxide concentration history for EGR=21% and EGR=34%. It presents that when higher EGR is applied, value of NO formation decreases.

Figure 4- 13 shows the soot density history for EGR=21% and 34%. And when the higher EGR is applied, soot emission increases.

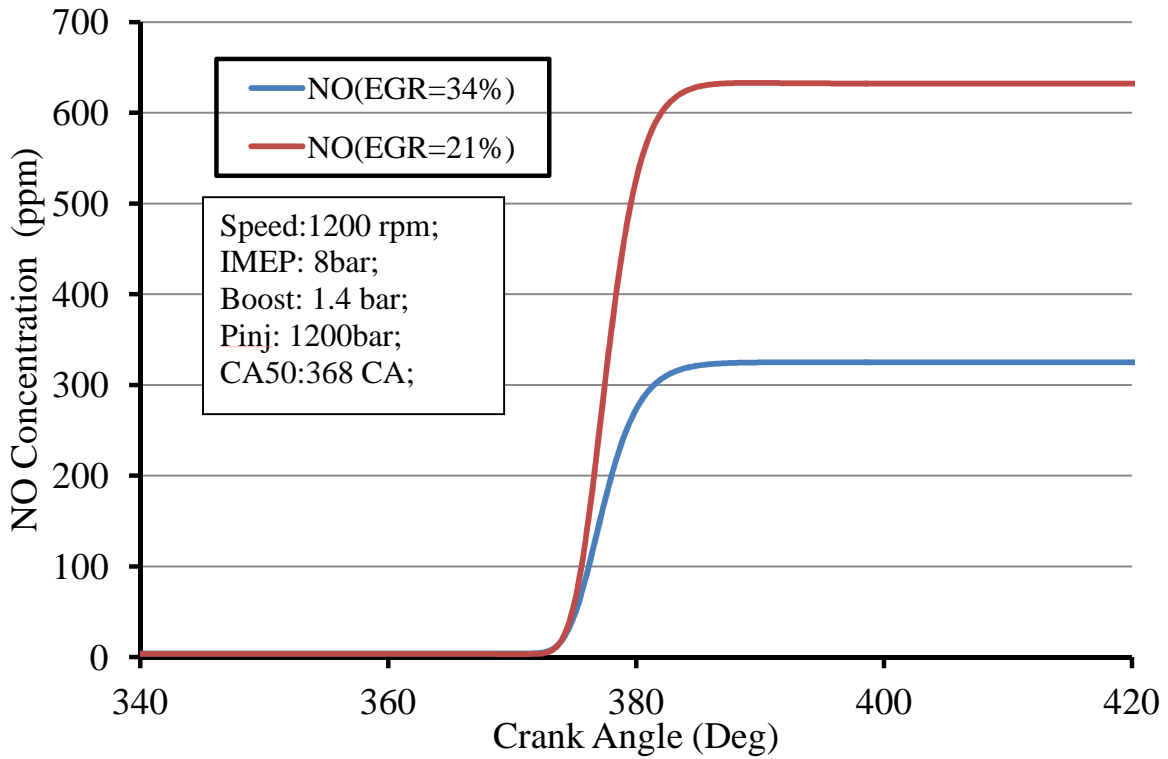


Figure 4- 12 Calculated and measured in-cylinder Nitric Oxide (NO) concentration

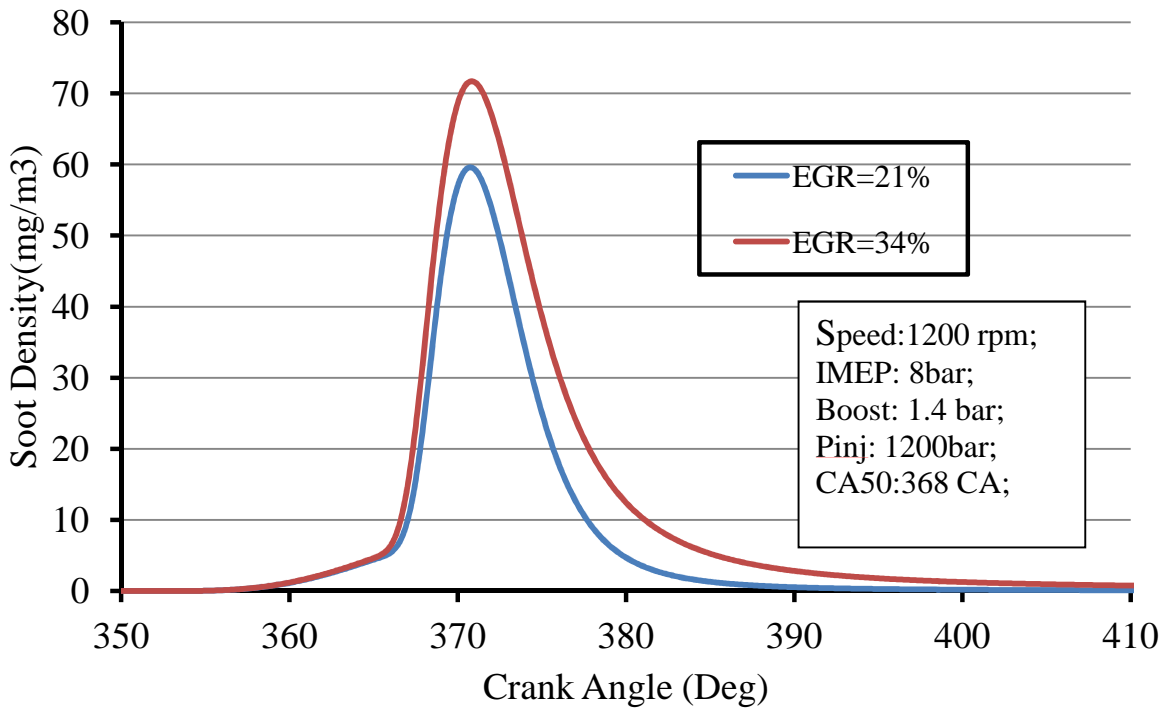


Figure 4- 13 Calculated and measured in-cylinder soot concentration

EGR is one of the most effective ways to reduce NO<sub>x</sub> emission for diesel engines. From Figure 4- 14, it can be observed that the NO<sub>x</sub> decreases when higher EGR rate is applied under fixed operating condition. It is hard to simulate the diesel engine combustion process and precisely predict the emission. But for the control purpose, as it can be observed, this model presents high reliability to predict the trend and relative change in NO emissions within different operating conditions.

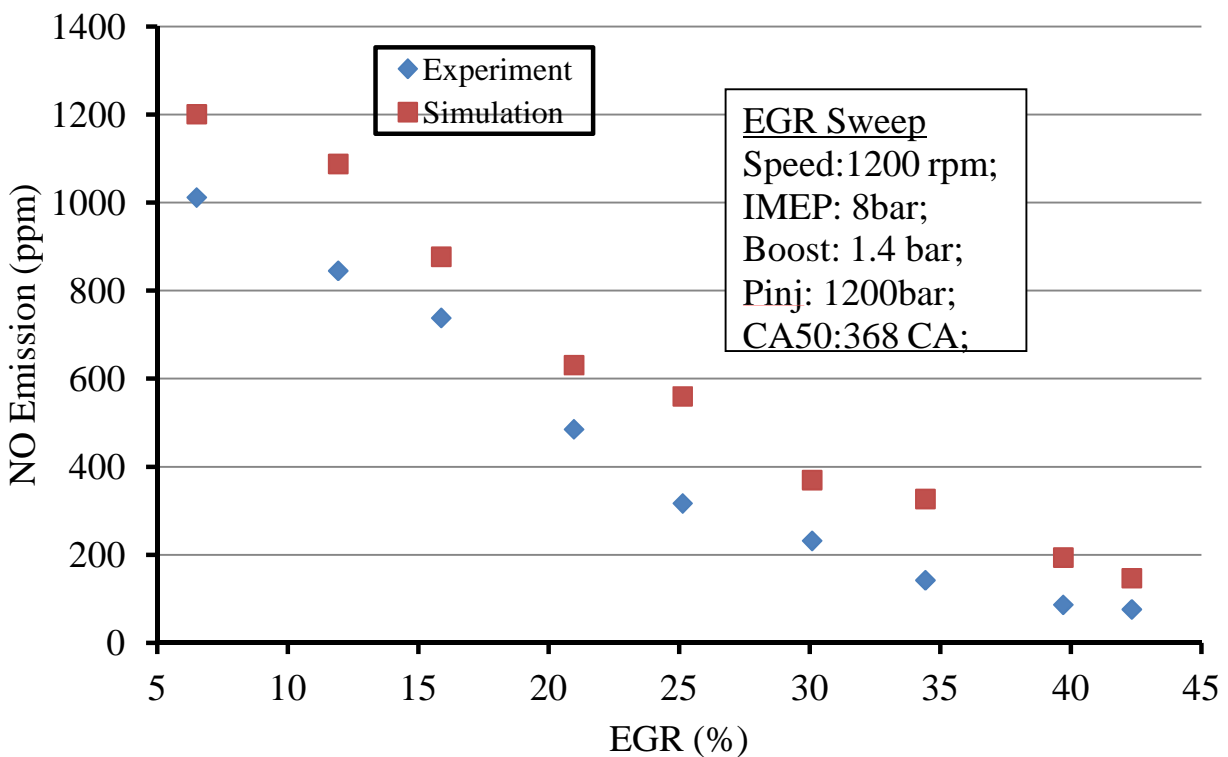


Figure 4- 14 Calculated and measured in-cylinder Nitric Oxide (NO) formation

Figure 4-15 illustrates the comparison of the simulated and measured soot density when EGR rate increases from 15% to 45%. Soot formation is primarily determined by the engine load [9]. When the load increases, larger amount of fuel is injected into cylinders, which results in the increased temperature during the mixing controlled combustion [47].

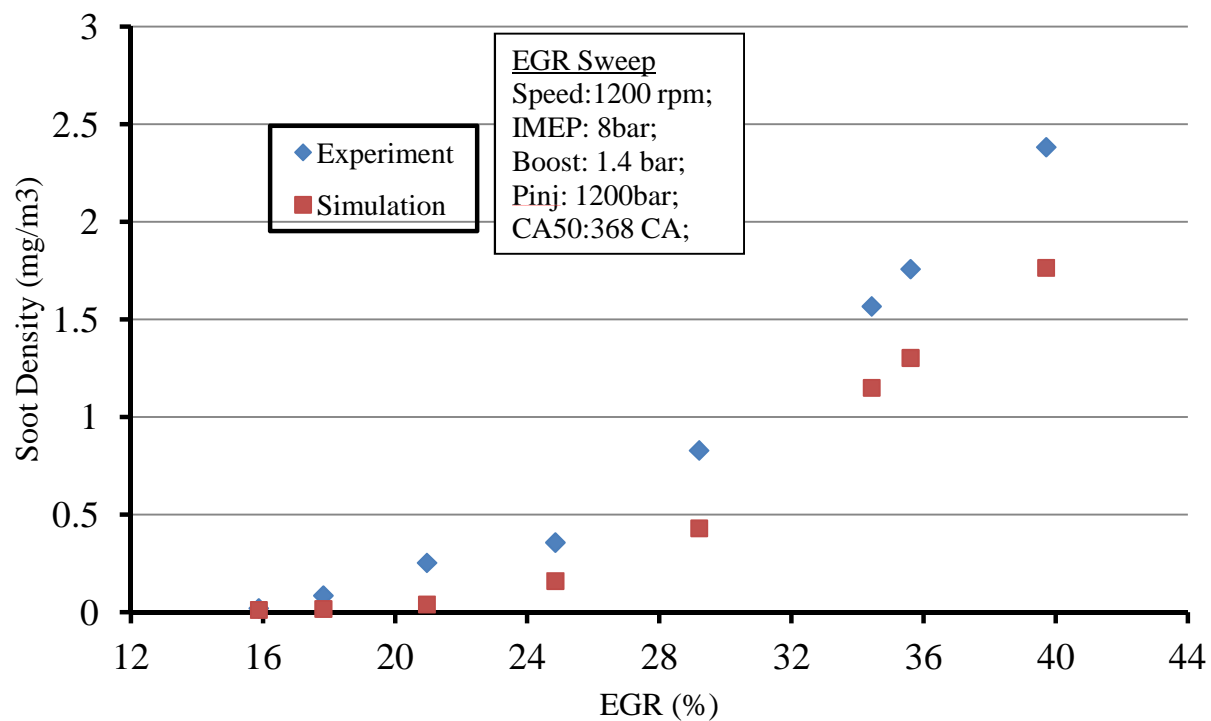


Figure 4- 15 Calculated and measured in-cylinder Nitric Oxide (NO) formation

## CHAPTER 5 APPLICATION OF ESTIMATION RESULTS TO SMART DIESEL ENGINE

After the calculation results of thermodynamic model and NO and soot emission estimation have been validated, the computation results of the 8 operating points will be shown in this chapter for the development of the engine-generator set controller design. The good agreement achieved in Chapter 4 between the empirical and calculated results under certain engine operating condition confirmed that the estimation will provide valuable information for the engine-generator control design. Table 5-1 presents the specification of the smart engine used for the engine-generator control design.

Table 5- 1 Smart Engine Specification

|                          |                                  |
|--------------------------|----------------------------------|
| Engine Type              | 3 in line,4 Stroke Diesel Engine |
| Bore (mm)                | 65.5                             |
| Stroke (mm)              | 79                               |
| Compression Ratio        | 18                               |
| Cylinder Displacement(L) | 0.8                              |
| Rated Torque (lb-ft)     | 95                               |
| Fuel Injection System    | Common Rail High Pressure        |





Figure 5- 1 Smart Car Cdi Engine

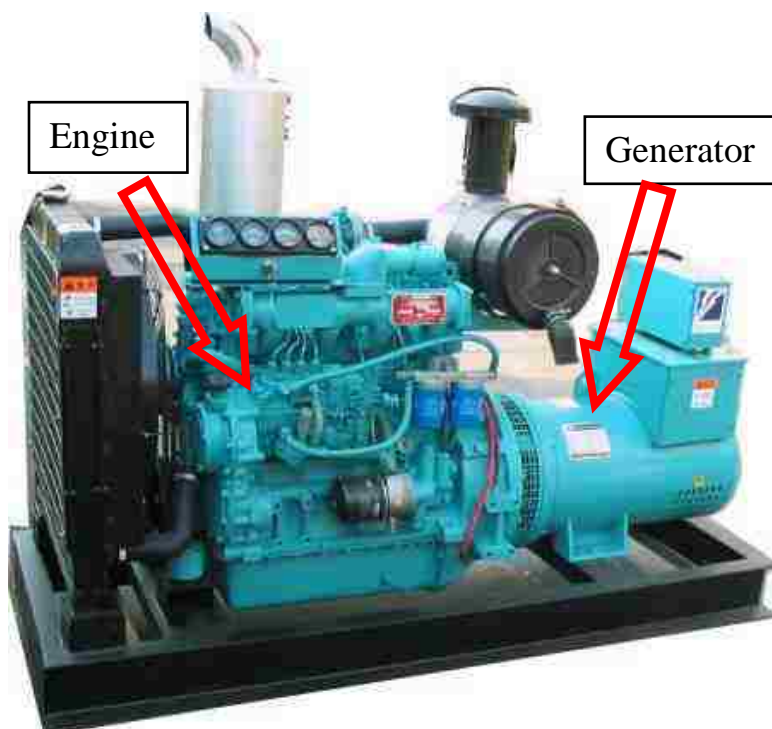


Figure 5- 2 Photo of engine-generator set (Courtesy Ricardo)

Table 5-2 shows the detailed information about the 8 operating points for the engine controller design. The speed ranges from 1600 rpm to 2800 rpm and the torque, output power and fuel flow all increase as well.

Table 5- 2 Detailed Information about 8 Operating Points

| Operating Point | Engine Speed (rpm) | Torque (Nm) | Power (kW) | Fuel Flow (g/s) | Efficiency (%) | BMEP (bar) | CA 50 |
|-----------------|--------------------|-------------|------------|-----------------|----------------|------------|-------|
| #1              | 1600               | 42          | 7          | 0.51            | 0.33           | 6.6        | 365   |
| #2              | 1950               | 51          | 10         | 0.72            | 0.345          | 8.0        | 365   |
| #3              | 2150               | 58          | 13         | 0.89            | 0.35           | 9.1        | 365   |
| #4              | 2250               | 67          | 16         | 1.07            | 0.352          | 10.5       | 365   |
| #5              | 2450               | 75          | 19         | 1.31            | 0.351          | 11.8       | 365   |
| #6              | 2570               | 82          | 22         | 1.52            | 0.345          | 12.9       | 365   |
| #7              | 2630               | 90          | 25         | 1.75            | 0.337          | 14.1       | 365   |
| #8              | 2800               | 95          | 28         | 2.05            | 0.324          | 14.9       | 365   |

The following figures show the benefit of EGR in reducing of NO<sub>x</sub> emission for the eight operating points. It can be seen that with the increase of EGR rate, the NO emission decreases under all of the eight different operating conditions. In general, there are two reasons which can explain relationship between NO<sub>x</sub> formation and EGR rate. The first reason for NO<sub>x</sub> emission reduction with higher EGR is because that the higher the values of the EGR rate that is used, the lower the in-cylinder temperature during combustion process. The second reason is the reduction of oxygen concentration which restrains NO<sub>x</sub> generation. As mentioned previously, NO<sub>x</sub> emission is very sensitive to temperature and oxygen concentration.

To study the EGR effect on the engine performance and emission, for each operating point, certain parameters will be fixed, such as engine speed, injected fuel quality, intake pressure and temperature.

Figure 5- 3 shows the typical effect of EGR on the NO<sub>x</sub> formation for operating point 1, 2, 3 and 4. For operating point 1, NO<sub>x</sub> formation is reduced drastically with 12% EGR. For operating point 2, it is reduced by approximately 70% within 15% EGR.

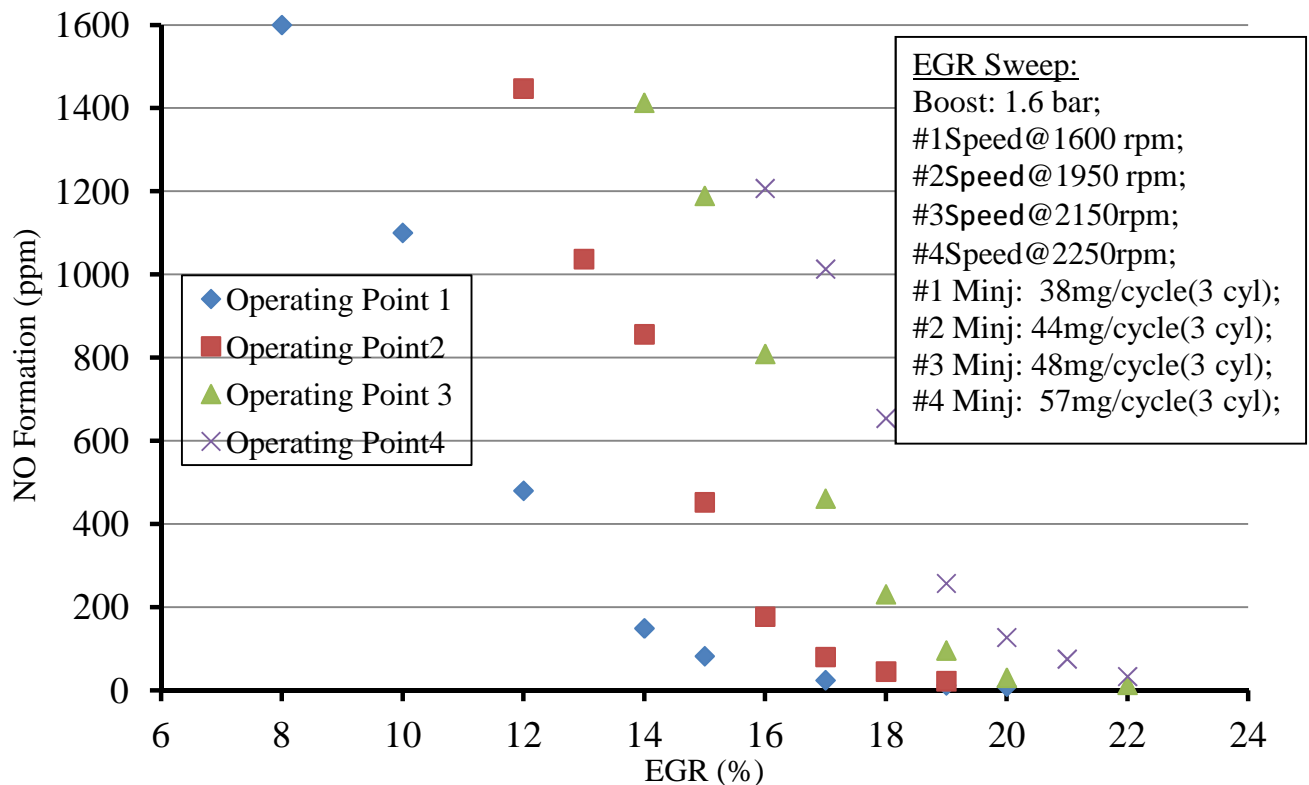


Figure 5- 3 Relationship between EGR and NO<sub>x</sub> formation (for Operating Point 1-4)

From the simulation results, we can see that from operating point 5 to 8, the NO emissions are relatively high. Thus we require a higher EGR. For example, with the increase of the amount of fuel injection, for operating point 5, when EGR is 20%, the NO emission is around 1200 ppm, but for operating point 3, when EGR is increased to 20%, there is almost no NO<sub>x</sub> present.

Figure 5- 4 shows the relationship between NO formation and EGR rate of operating point #5, #6 and #7 when boost is increased from 1.6 bar to 2 bar. Comparing with Figure 5- 3, in the case of operating point #5, 6 and 7, the engine is running in a higher load and speed. Therefore higher EGR rate and boost are required.

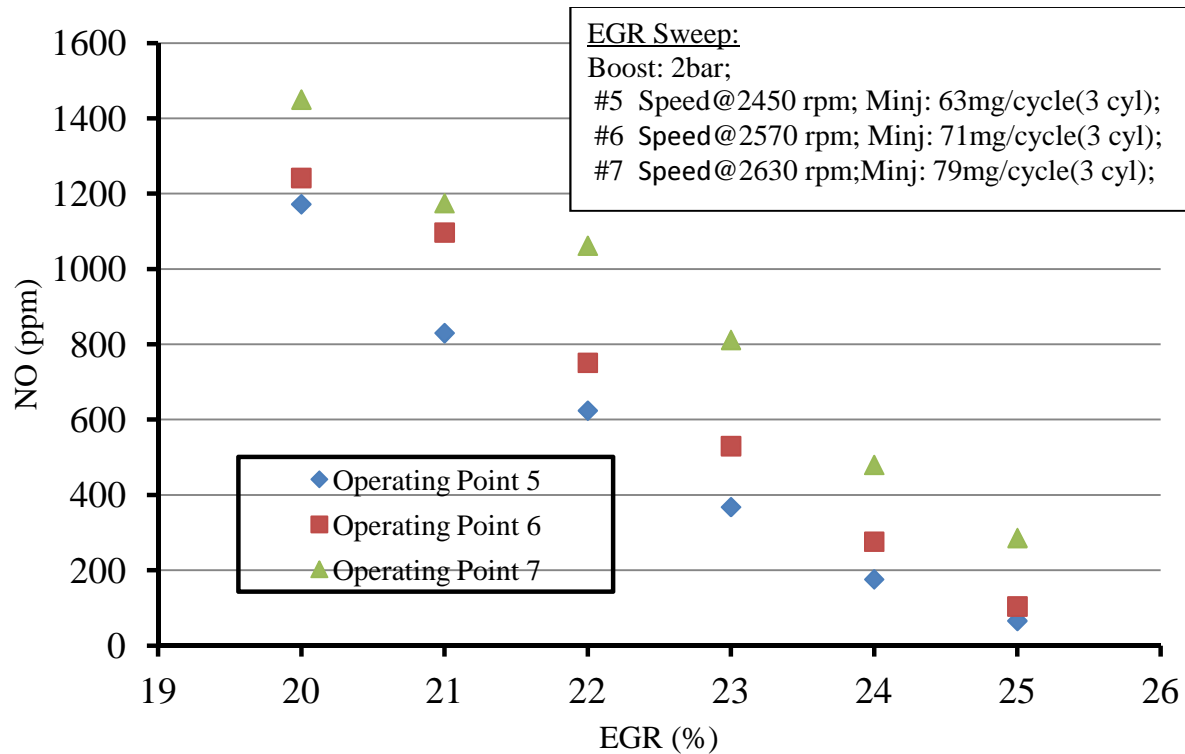


Figure 5- 4 Relationship between EGR and NOx formation (for Operating Point 5-7)

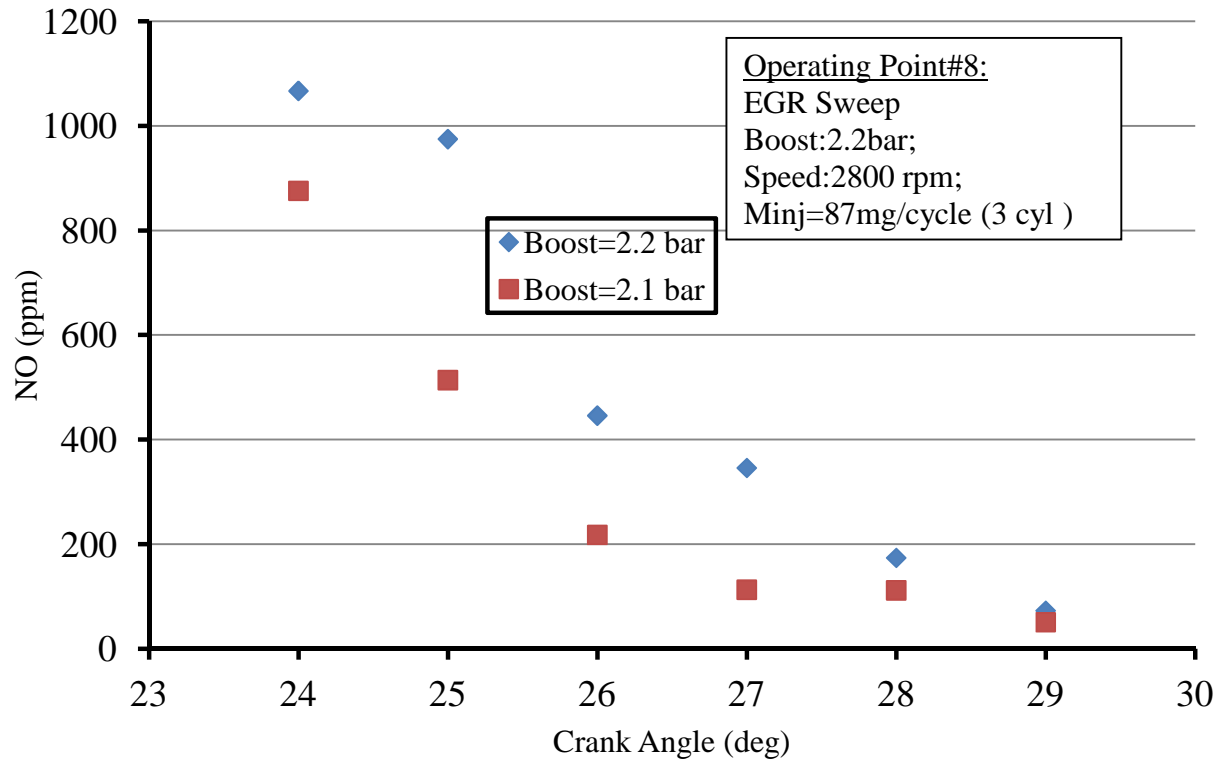


Figure 5- 5 Relationship between EGR and NOx formation (for Operating Point 8)

Figure 5- 6 and Figure 5- 7 show the calculation results for soot emissions which all follow the same trend with various EGR rates. With the increase of EGR, soot emissions increase. This is because when the amount of fuel injected into cylinder increases, more fresh air is required to complete the combustion process. As it is shown in Figure 5- 6, for operating point 1, the fuel injection is around 38.1 mg/cycle, when EGR is 17% soot emission is around 2 mg/m<sup>3</sup>. But when the fuel injection increases to 64 mg/cycle, when EGR is increased to 19%, the soot emission is already over 6 mg/m<sup>3</sup>.

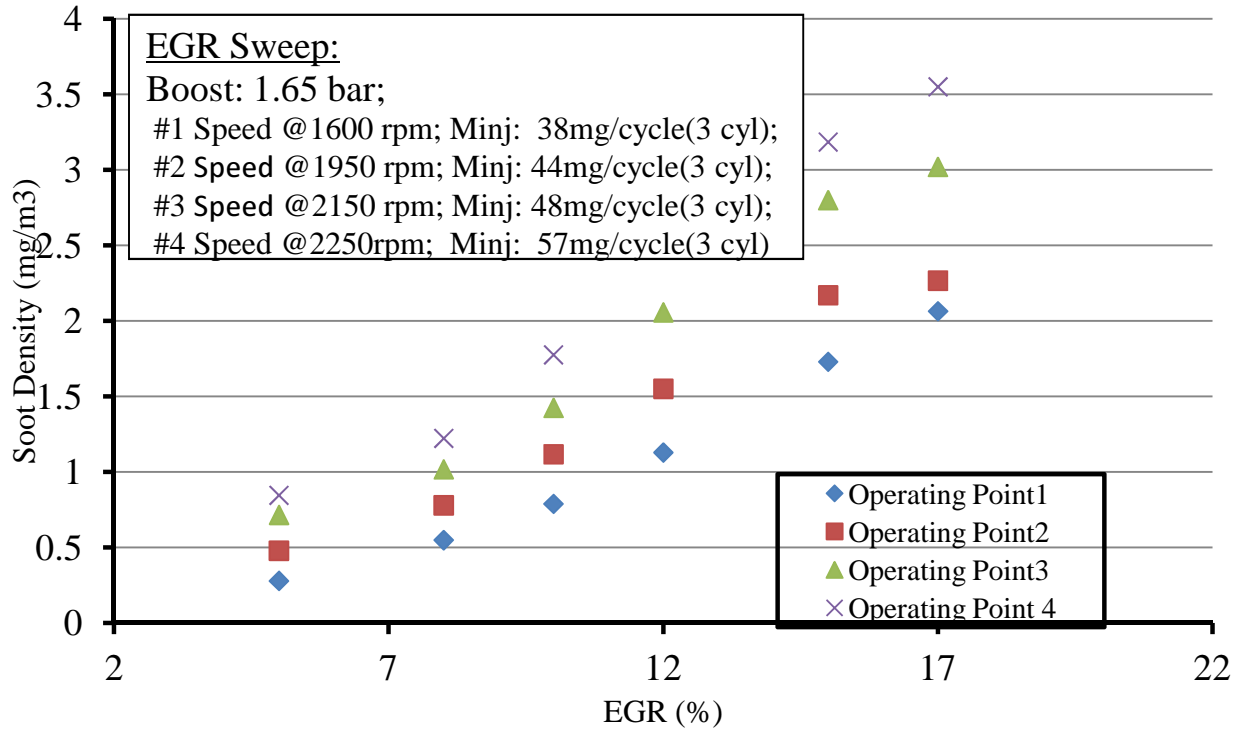


Figure 5- 6 Relationship between EGR and soot density (for Operating Point 1-4)

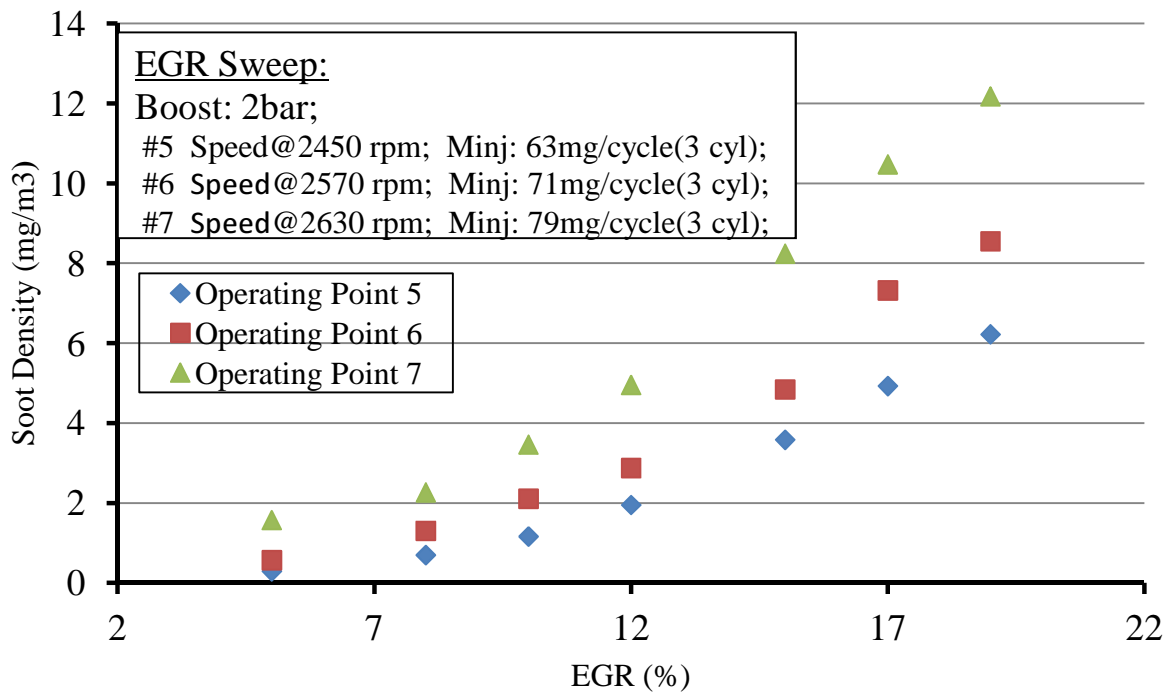


Figure 5- 7 Relationship between EGR and soot density (for Operating Point 5-7)

For operating point #8, the engine is working at 2800 rpm and the fuel injection quantity is increased to 87 mg/cycle. Figure 5- 8 and Figure 5-5 present the variation of soot and NO<sub>x</sub> formation with various EGR rates. When higher boost is applied to engine, higher NO<sub>x</sub> and lower soot density are achieved. The reason for the increase on the NO<sub>x</sub> formation and the reduction of soot formation is owing to excess air.

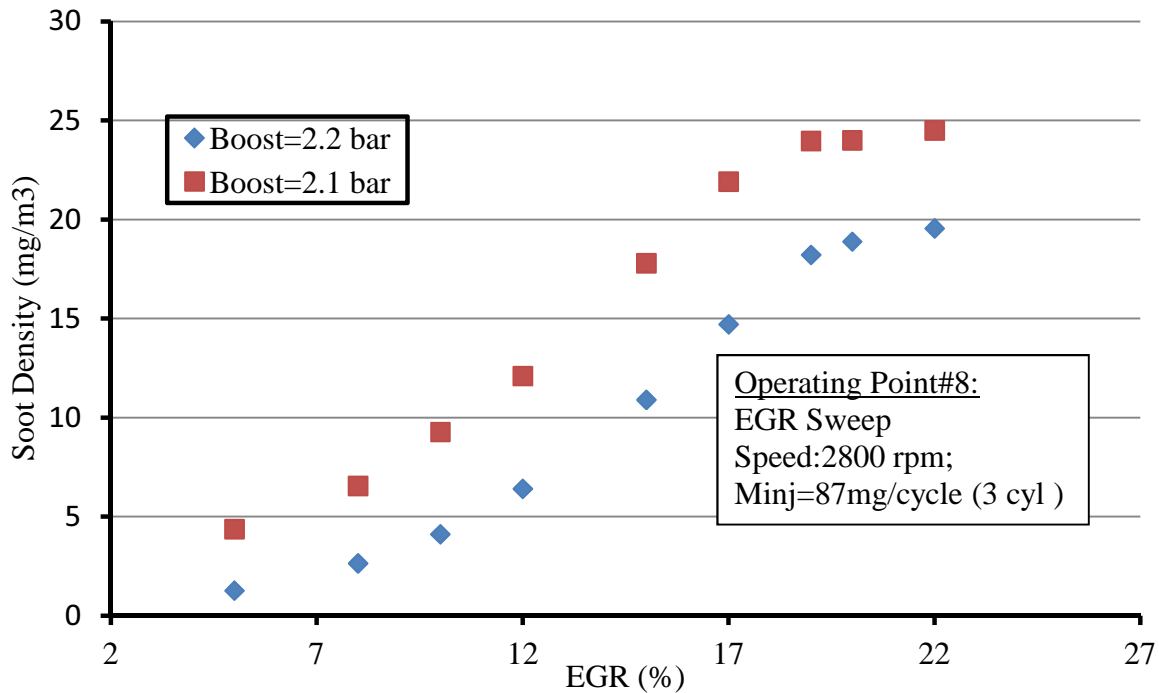


Figure 5- 8 Relationship between EGR and soot density (for Operating Point 8)

Figure 5- 9 and Figure 5-10 illustrate the in-cylinder pressure trace calculated under the condition of operating point 3 and 8 with different EGR rates. It shows the peak of in-cylinder pressure has decreased with the increase of EGR rates and the combustion timing has been retarded in these two cases.

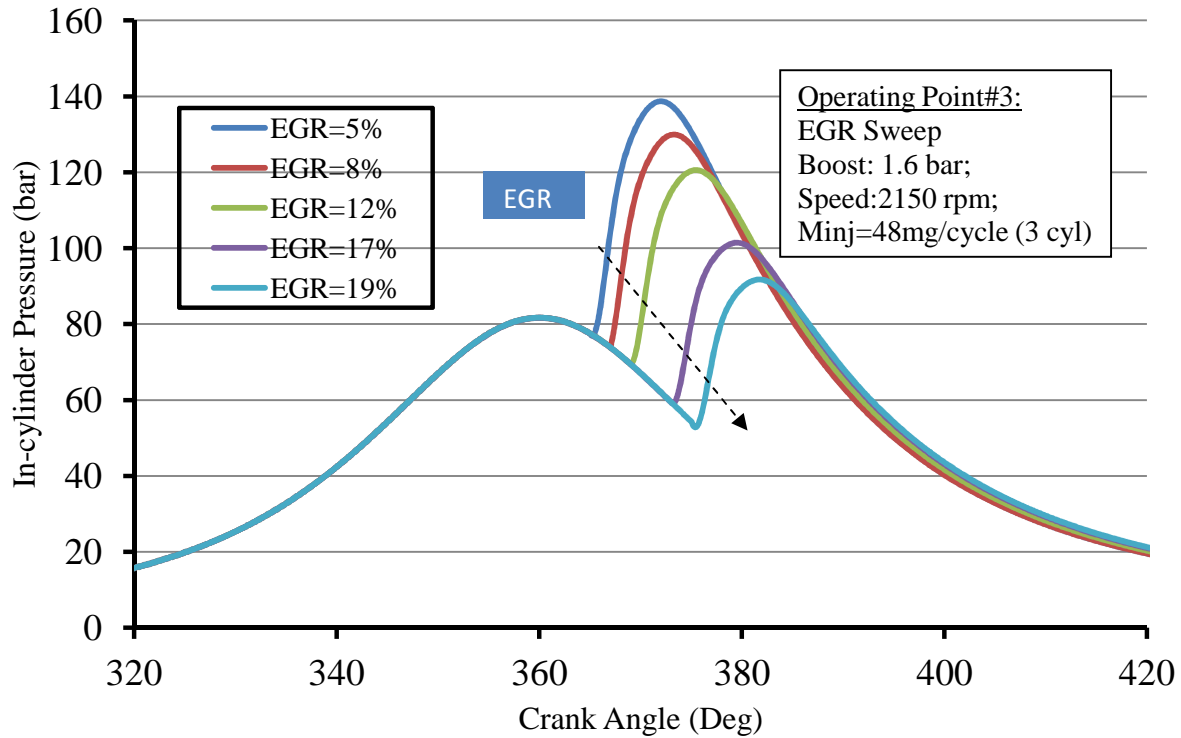


Figure 5- 9 In-cylinder pressure traces with different EGR rates (Operating Point 3)

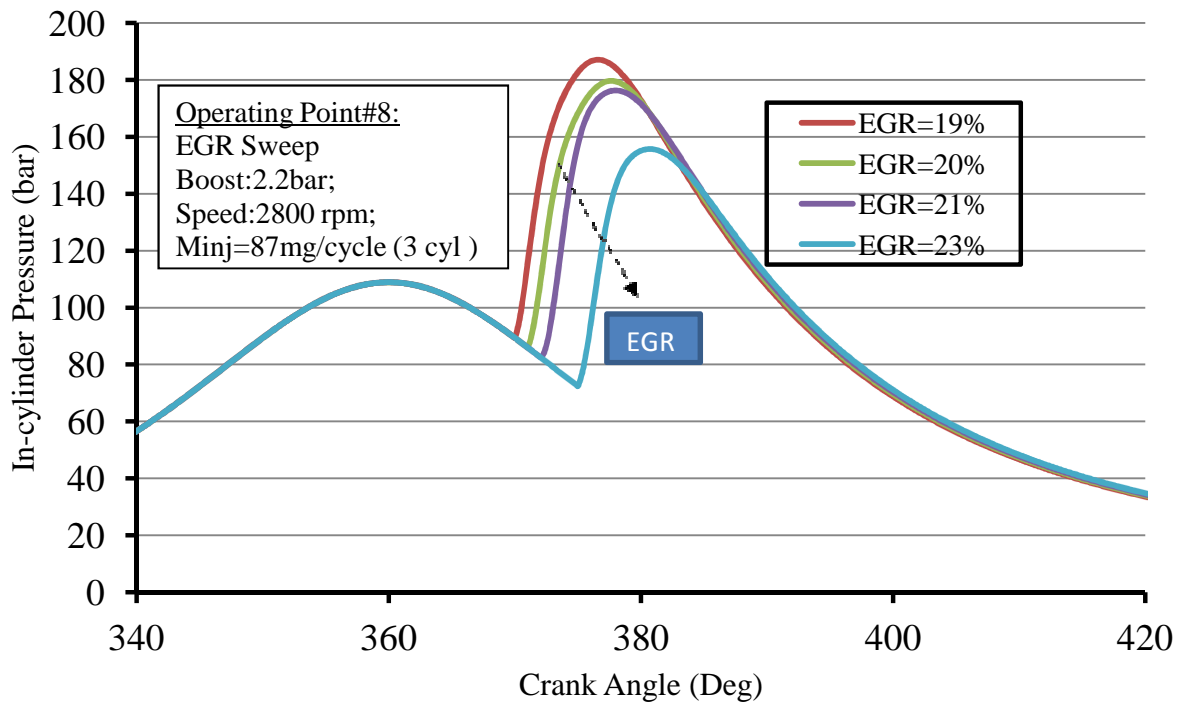


Figure 5- 10 In-cylinder pressure traces with different EGR rates (Operating Point 8)



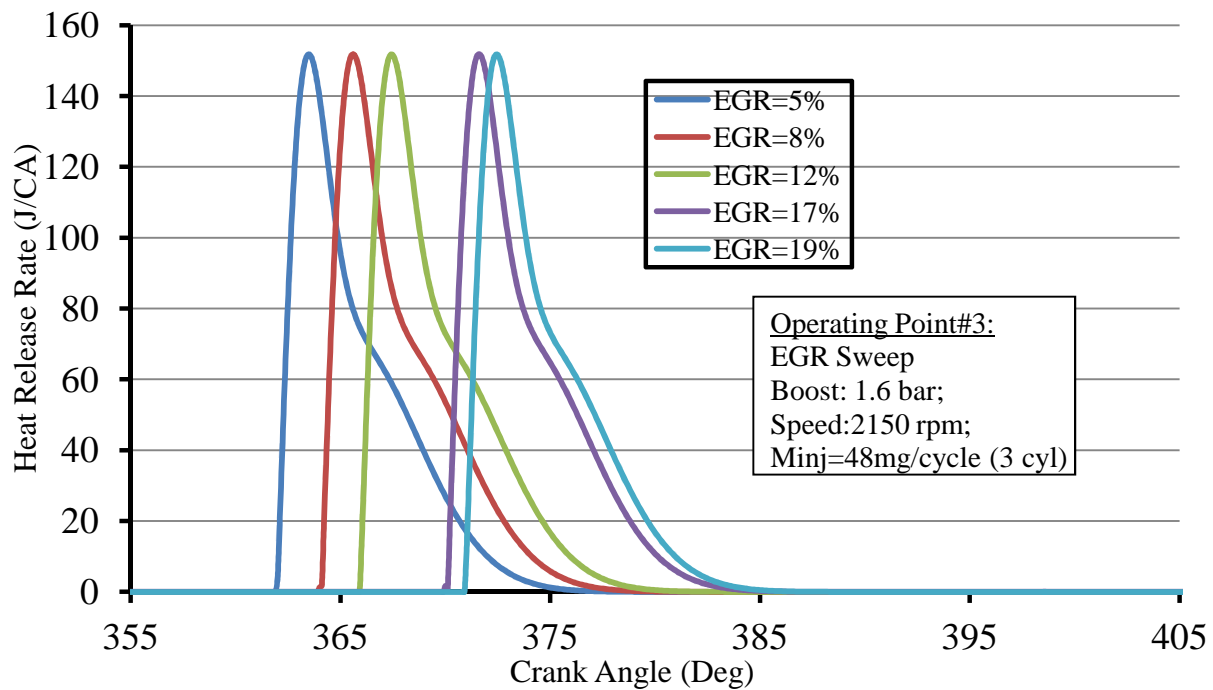


Figure 5- 11 Heat release rate with different EGR rates (Operating Point 3)

Figure 5- 12 illustrates the effect of EGR on ignition delay. The ignition delay increases with increasing EGR rate. The reason is that higher EGR results in lower oxygen concentration in the intake mixture, which will slow down the oxidation processes and increase ignition delay.

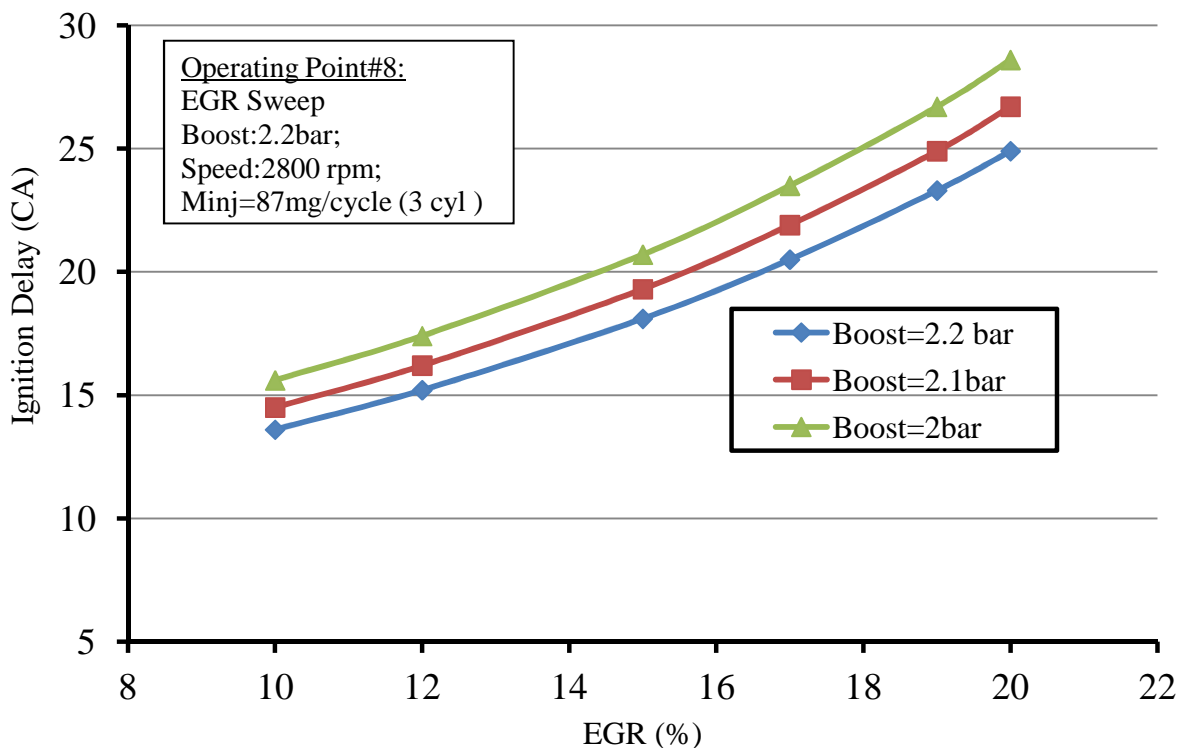


Figure 5- 12 Effect of boost on ignition delay

Figure 5- 13 illustrates the effect of the intake oxygen concentration and injection timing on the in-cylinder peak pressure for operating point 1. With the same injection timing, the in-cylinder peak pressure increases when intake oxygen concentration increases. For the in-cylinder combustion, higher oxygen concentration is equivalent to lower  $\text{CO}_2$  concentration, which results in the decrease of specific heat capacity and the increase of in-cylinder temperatures. Therefore the in-cylinder peak pressures increase. With the same intake oxygen concentration, the in-cylinder peak pressure decreases when the injection timing is retarded. For example, when the injecting timing is at -9 CA ATDC and the oxygen concentration is below 18%, combustion did not occur. But when the injecting timing is at -20 CA ATDC, the low limit of oxygen concentration is 17%.

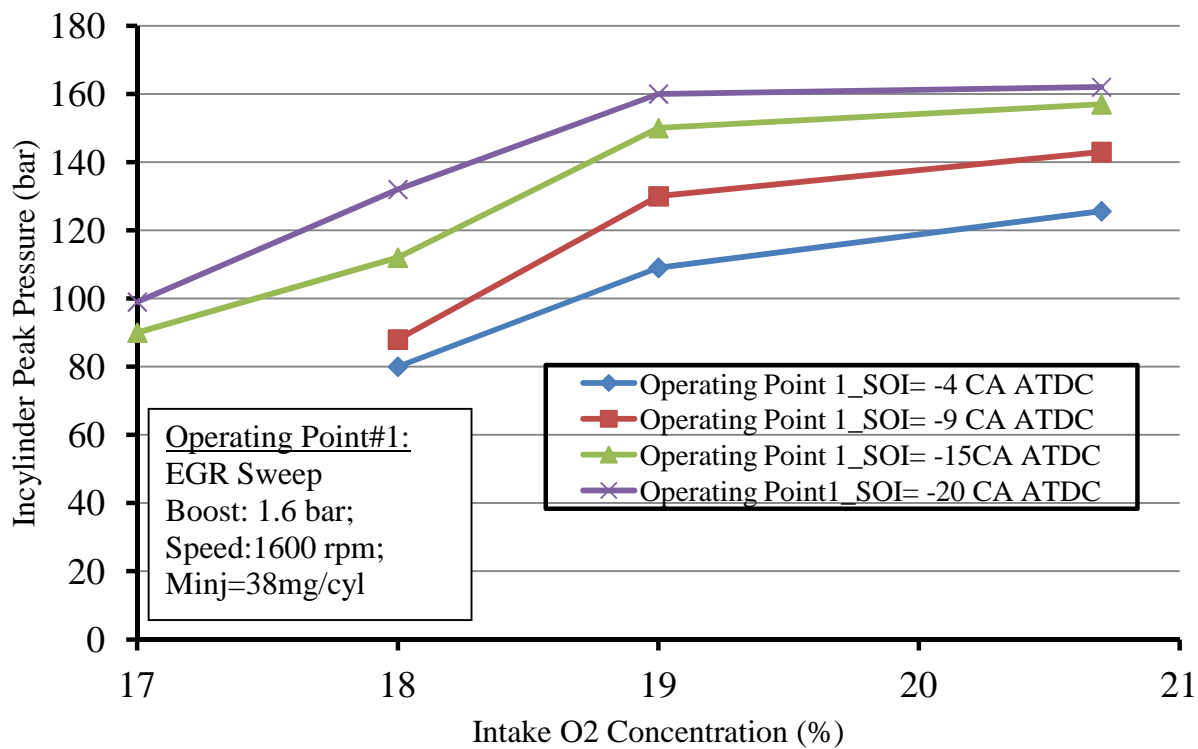


Figure 5- 13 Effect of intake Oxygen concentration on the in-cylinder peak pressure

## **CHAPTER 6 CONCLUSION AND FUTURE WORK**

### **6.1 Conclusion**

The objective models for emission estimation for a series PEHV diesel engine-generator set control design, which combine the thermodynamic engine model, NO<sub>x</sub> model, soot model and EGR model described in Chapter One, have been developed. The heat release model was tuned to match the empirical data until the satisfactory results have been achieved, and the calculated in-cylinder pressure agrees well with the experimental data. Furthermore, the in-cylinder temperature, heat release rate, species mole fraction were calculated and provided as the inputs of the NO<sub>x</sub> and soot emission estimation models. Comparing to the previous work, the emission estimation model has been modified to take EGR system into account. Additionally, the NO<sub>x</sub> and soot emission estimation was validated and satisfactory for the Diesel engine-generator set control design. According to the implemented Model Predictive Control (MPC) design, eight operating points were selected to represent the diesel engine output power ranging from 7kW to 28kW. And the NO and soot emission results with EGR sweep for each operating point were provided for the diesel engine-generator controller design.

### **6.2 Future Work**

In the validation part, more EGR sweep experiments shall be further conducted with various boundary operating conditions. Measured experimental data from Clean Diesel Engine Lab was satisfactory for certain limited operating range. More empirical data collected will bring improvement over the previous validation work.

The next stage of the research shall target on a two-zone thermodynamic engine model. NO<sub>x</sub> emission is very sensitive to the in-cylinder temperature and oxygen concentration. For the engine control application, the single zone dynamic engine model had been efficient to accomplish the estimation work. However, when the two-zone engine model is applied to the emission estimation model, it will provide more accurate prediction.

## REFERENCES

- [1] Chan-Chiao Lin, “Modeling and Control Strategy Development for Hybrid Vehicles”, PhD Dissertation, University of Michigan, 2004.
- [2] Richard J. Asay, “A Five-Zone Model for Direct Injection Diesel Combustion”, Master Thesis, Brigham Young University, 2003.
- [3] Phillip S. Sharer, Aymeric Rousseau, Dominik Karbowski and Sylvain Pagerit, “Plug-in Hybrid Electric Vehicle Control Strategy: Comparison between EV and Charge-Depleting Options”, SAE International paper No. 2008-01-0460, 2008.
- [4] David E. Smith, Henning Lohse-Busch and David K. Irick, “A Preliminary Investigation into the Mitigation of Plug-in Hybrid Electric Vehicle Tailpipe Emissions Through Supervisory Control Methods Part 1: Analytical Development of Energy Management Strategies”, SAE International paper No. 2010-01-1266, 2010.
- [5] Oliver Grondin, Laurent Thibault, Philippe Moulin, Alexander Chasse and Antonio Sciattetta, “Energy Management Strategy for Diesel Hybrid Electric Vehicle”, Vehicle Power and Propulsion Conference (VPPC), Chicago, IL, 2011 IEEE.
- [6] Sherry Boschert, “Well-to-wheels Emissions Data for Plug-in Hybrids and Electric Vehicles: An Review”, New Society Publishers, 2006.
- [7] “Emission Estimation Technique Manual for Combustion Engines Version 2.2”, National Pollutant Inventory, 2002
- [8] Reed M. Benet, “Better Than Ethanol? BTL in Plug-in Hybrid Diesel Vehicles”, Google Tech Talks September 20, 2006.
- [9] John B. Heywood, “Internal Combustion Engine Fundamentals”, McGraw-Hill, Singapore,

---

1988.

- [10]“Emission Estimation Technique Manual for Combustion Engines Version 3.0”, National Pollutant Inventory, <http://www.npi.gov.au/publications/emission-estimation-technique/pubs/combustion-engines.pdf>, 2008.
- [11]Robert Joumard, “Methods of Estimation of Atmospheric Emissions from Transport: European Scientist Network and Scientific State-of –the art action COST 319 final report”, <http://www.alpnep.org/C319finalreport.pdf> ,March 1999
- [12]C.D. Rakopoulos, K. A. Antonopoulos, D.C. Rakopoulos and D.T. Hountalas, “Multi-zone Modeling of Combustion and Emissions Formation in DI Diesel Operating on Ethanol-diesel Fuel Blends ”, *Energy Conversion and Management* 49 (4) :625-643,2008,  
DOI: 10.1016/j.enconman.2007.07.035
- [13]Pia Kilpinen; “Optimization of a Simplified Sub-model for NO Emission Prediction by CFD in Large 4-stroke Marine Diesel Engines”, *Fuel Processing Technology* 91(2):18-228, February 2010.
- [14]Z.S. Filipi and D.N. Assanis, “A Nonlinear Transient, Single-Cylinder Diesel Engine Simulation for Predictions of Instantaneous Engine Speed and Torque” , *ASME J. Eng. Gas Turbines Power* 123(4) 951(9 pages), 2001  
DOI:10.1115/1.1365122
- [15]Y H Zweiri, J F Whidborne and L D Seneviratne, “Detailed Analytical Model of a Single-Cylinder Diesel Engine in the Crank Angle Domain”, *Journal Automobile Engineering* 215(11):1197-1216, 2001.
- [16]Zehra Sahin and Orhan Durgun, “Multi-zone Combustion Modeling for the Prediction of Diesel Engine Cycles and Engine Performance Parameters”, *Applied Thermal Engineering*28 (17-18):2245-2256, 2008.

---

DOI:10.1016/j.applthermaleng.2008.01.002

- [17] A Chow and M L Wyszynski, "Thermodynamic Modeling of Complete Engine Systems-a Review", Journal of Automobile Engineering 213(4):213- 403, 1999.
- [18] R. Miller, G. Davis, G. Lavoie and C. Newman, "A Super-Extended Zeldovich Mechanism for NO<sub>x</sub> Modeling and Engine Calibration", SAE international, 980781, 1988.
- [19] Sundar R. Krishnan, Kalyan K. Srinivasan and K. Clark Midkiff, "Modeling of NO<sub>x</sub> Emissions Using a Super-Extend Zeldovich Mechanism", ASME 2003 Internal Combustion Engine and Rail Transportation Divisions Fall Technical Conference (ICERT) Paper No. ICEF2003-713.
- [20] Edgardo Coda Zabetta and Pia Kilpinen, "Improved NO<sub>x</sub> Submodel for In-Cylinder CFD Simulation and Low-and Medium –Speed Compression Ignition Engines", Energy & Fuels 15(6):1425-1433, 2001.
- [21] Feng Tao, Valeri I. Golovichev and Jerzy Chomalik, "A Phenomenological Model for the Prediction of Soot Formation in Diesel Spray Combustion", Combustion and Flame 136 (3)270-282, 2004.
- DOI:10.1016/j.combustflame.2003.11.001
- [22] Z.A. Mansurov, "Soot Formation in Combustion Processes" Combustion, Explosion and Shock Waves 41(6):727-744, 1994.
- DOI: 10.1007/s10573-005-0083-2
- [23] Lakshminarayanan, P.A and Aghav, Y.V, "Modelling Diesel Combustion", Technology & Engineering, 2010.
- [24] Anders Westlund, "Fast Physical Prediction of NO and Soot in Diesel Engines", SAE International paper No. 2009-01-1121, 2009.



- 
- [25] Niklas Winkler and Angstrom H-E, "Simulations and Measurements of a two-stage Turbocharged Heavy-duty Diesel Engine Including EGR in Transient Operation", SAE paper No. 2008-01-0539, 2008.
- [26] Joan Boulanger, Fengshan Liu, W. Stuart Neill and Gregory J. Smallwood, "An Improved Soot Formation Model for 3D Diesel Engine Simulations", Journal of Engineering for Gas Turbines and Power 129(3)(8 pages), 2007.
- DOI:10.1115/1.2718234
- [27] "Technology Roadmap: Electric and Plug-in Hybrid Electric Vehicles", International Energy Agency, [http://www.iea.org/papers/2009/EV\\_PHEV\\_Roadmap.pdf](http://www.iea.org/papers/2009/EV_PHEV_Roadmap.pdf), July 2011;
- [28] A. Santos, N. McGuckin, H.Y. Nakamoto, D. Gray and S. Liss, "Summary of Travel Trends: 2009 National Household Travel Survey", U.S. Department of Transportation, report No., FHWA-PL-11-022, June 2011;
- [29] Aymeric Rousseau and Ayman Moawad, "Impact of Control Strategies on Fuel Efficiency of Different PHEVs Using Real World Driving Conditions", Argonne National Laboratory, <http://www.transportation.anl.gov/pdfs/HV/570.pdf>, 2009.
- [30] Maxime Pasquier and Gilles Monnet, "Diesel Hybridization and Emissions –A Report to DOE from the ANL Vehicle Systems and Fuels Team", Argonne National Laboratory, <http://www.transportation.anl.gov/pdfs/HV/324.pdf>.
- [31] Vincent Freyermuth, Eric Fallas and Aymeric Rousseau, "Comparison of Powertrain Configuration for Plug-in HEVs from a Fuel Economy Perspective". SAE International paper No. 2008-01-0461, 2008.
- [32] Stan Liviu Constantin and Mitu Daniela-elena. "Simplified Mechanism Used to Estimate the NOx Emission of Diesel Engine", 2<sup>nd</sup> International Conference on Manufacturing Engineering, Quality and Production Systems, 2010.

- 
- [33] Hongsuk Kim and Nakwon Sung, "Multidimensional Engine Modeling: NO and Soot Emissions in Diesel Engine With Exhaust Gas Recirculation", *KSME International Journal*, 15 (8):1196-1204, 2001.,
- [34] Yunus A. Gengel and Michael A. Boles, "Thermodynamics: An Engineering Approach", McGraw-Hill, Europe, 2006.
- [35] Timothy Jacobs, Dennis Assanis, and Zoran Filipi; "The impact of Exhaust Gas Recirculation on Performance and Emissions of a Heavy-Duty Diesel Engine", SAE paper No. 2003-01-1068, 2003.
- [36] N Ladommatos, S Abdhalim and H Zhao. "The effect of the Exhaust Gas Recirculation on Diesel Combustion and Emissions", *International Journal of Engine*, 1 (1): 107-126, 2000.
- [37] K. Boussouara and M. Kadja, "Numerical Investigation of Soot Formation in Diesel Jet Flame with KIVA-3V", *Revue des Energies Renouvelables* 12(1):22-62, 2009.
- [38] Anders Westlund, "Measuring and Predicting Transient Diesel Engine Emissions", PhD Dissertation, KTH Royal Institute of Technology, 2009.
- [39] Zhiyu Han, Ali Uludogan, Gregory J. Hampson and Rolf D. Reitz, "Mechanism of Soot and NO<sub>x</sub> Emission Reduction Using Multiple-Injection in a Diesel Engine", SAE International paper No. 960633, 1996.
- [40] C.D. Rakopoulos, K.A. Antomopoulos and D.C. Rakopoulos, "Development and Application of Multi-zone Model for Combustion and Pollutants Formation in Direct Injection Diesel Engine Running with Vegetable Oil or Its Bio-diesel", *Energy Conversion and Management*, 48( 7):1881-1901, July 2007.  
[DOI:10.1016/j.enconman.2007.01.026](https://doi.org/10.1016/j.enconman.2007.01.026)
- [41] C.O Schmalzing, P. Stapf, R. R. Maly and G. Renner, "A Holistic Hydraulic and Spray

- 
- Model –Liquid and Vapor Phase Penetration of Fuel Sprays in DI Diesel Engines”, SAE paper No.1999-01-3549,1999.
- DOI: 10.4271/1999-01-3549
- [42]H. Yasar, H.S. Soyhan, H. Walmsley, B. Head and C. Sorousbay; “Double-Wiebe Function: an Approach for Single-zone HCCI Engine Modeling”, Applied Thermal Engineering 28(11-12)1284-1290, 2008.
- DOI: 10.1016/j.applthermaleng.2007.10.014
- [43]Marcus Klein, “A Specific Heat Ratio Model and Compression Ratio Estimation”, Master Thesis, Linkoping University, 2004.
- [44]J I Ghojel, “Review of the Development and Applications of the Wiebe Function: a Tribute to the Contribution of Ivan Wiebe to Engine Research”, International Journal of Engine Research 11(4):297-312, 2010.
- [45]K. Alkhulaifi and M. Hamdalla, “Ignition Delay Correlation for a Direct Injection Diesel Engine Fuelled with Automotive Diesel and Water Emulsion”, World Academy of Science, Engineering and Technology, page 905, 2011.
- [46] Cyril Crua, “Combustion Processes in a Diesel Engine”, School of Engineering, PhD Dissertation, University of Brighton, 2002.
- [47]C.D. Rakopoulos, D.C. Rakopoulos, E.G. Giakomuis and D.C. Kyritsis, “Validation and Sensitivity Analysis of a Two Zone Diesel Engine Model for Combustion and Emissions Prediction”, Energy Conversion Management 45(9-10) 1471-1495, 2004.
- DOI:10.1016/j.enconman.2003.09.012
- [48] Arjun Krishnan and Vinay C. Sekar, “Prediction of NO<sub>x</sub> reduction with Exhaust Gas Recirculation Using the Flame Temperature Correlation Technique”, National Conference on

---

Advances in Mechanical Engineering, March 18-19,2006.

[49]Hanson RK and Salimian S, “Survey of rate constants in H/N/O System”, Combustion Chemistry, p.361, 1984.

[50]ANSYS FLUENT, “Fluent 6.3 Documentation”, Fluent Inc, 2006.

[51]J.J. Hernandez, M.Lapuerta, and J.Perez-Collado, “A Combustion Kinetic Model for Estimating Diesel Engine NO Emissions”, Combustion Theory and Modeling, 10(4):639-657, 2006.

[52] Nataporn Chindaprasert, “Thermodynamic Based Prediction Model for NOx and CO Emissions from a Gasoline Direct Injection Engine” PhD Dissertation, University of Rostock, 2007.

[53] Ming Zheng, Graham T. Reader and J. Gary Hawley, “Diesel Engine Exhaust Gas Recirculation-a Review on Advanced and Novel Concepts”, Energy Conversion and Management 45 (6) 883-900.

[DOI:10.1016/S0196-8904\(03\)00194-8](https://doi.org/10.1016/S0196-8904(03)00194-8)

[54]D.T. Hountalas, G.C. Mavropoulos and K.B. Binder, “Effect of Exhaust Gas Recirculation (EGR) Temperature for Various EGR Rates on Heavy Duty DI Diesel Engine Performance and Emissions”, Energy 33 (2) 272-283, 2008.

[DOI:10.1016/j.energy.2007.07.002](https://doi.org/10.1016/j.energy.2007.07.002)

## APPENDIX A. ESTIMATION RESULT VALIDATION

The comparison of experimental and simulation results of in-cylinder pressure with EGR=21% and EGR=34% was shown in Chapter 4. More validation results with various EGR rates will be illustrated in this section.

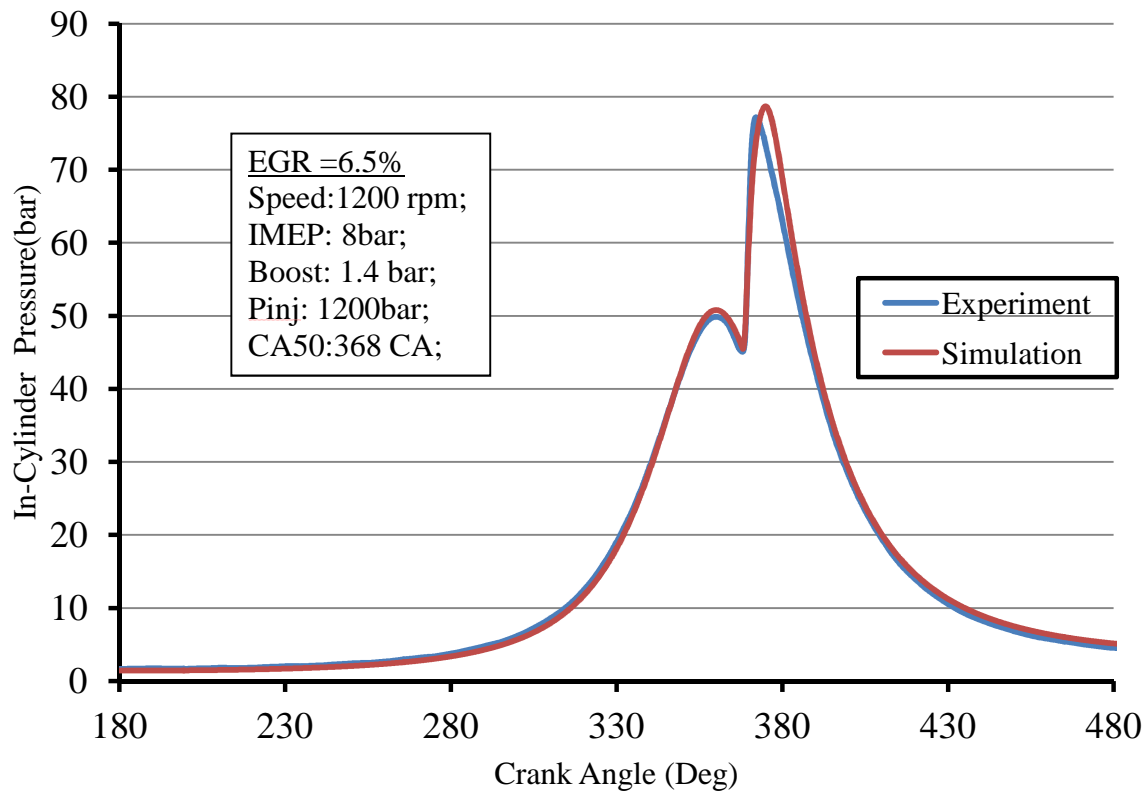


Figure A- 1 Comparison of the calculated and measured in-cylinder pressure (EGR=6.5%)

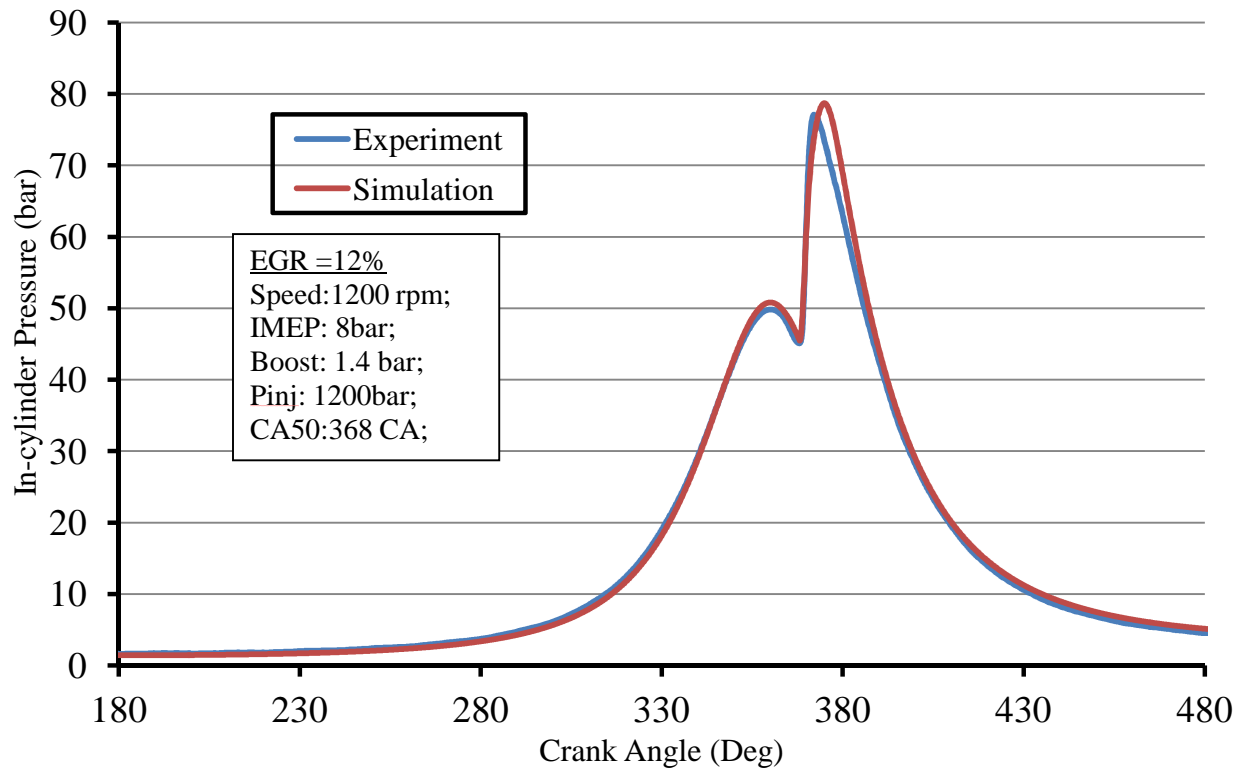


Figure A- 2 Comparison of the calculated and measured in-cylinder pressure (EGR=12%)

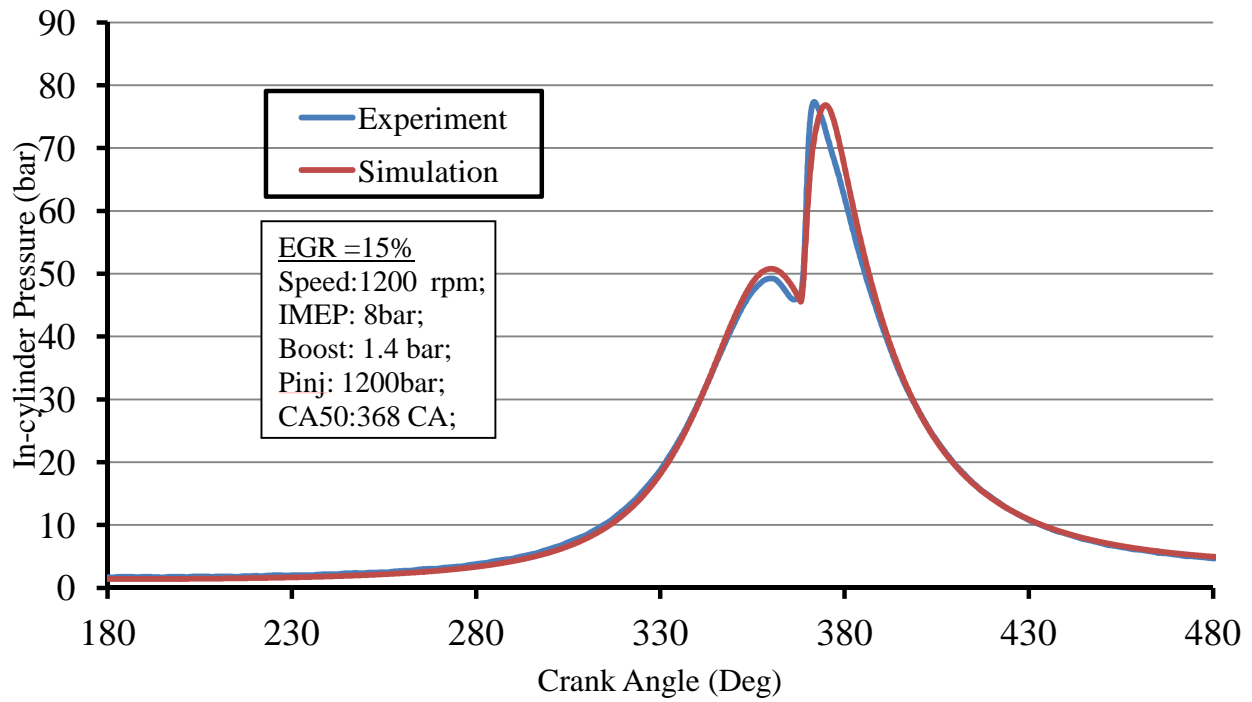


Figure A- 3 Comparison of the calculated and measured in-cylinder pressure (EGR=15%)

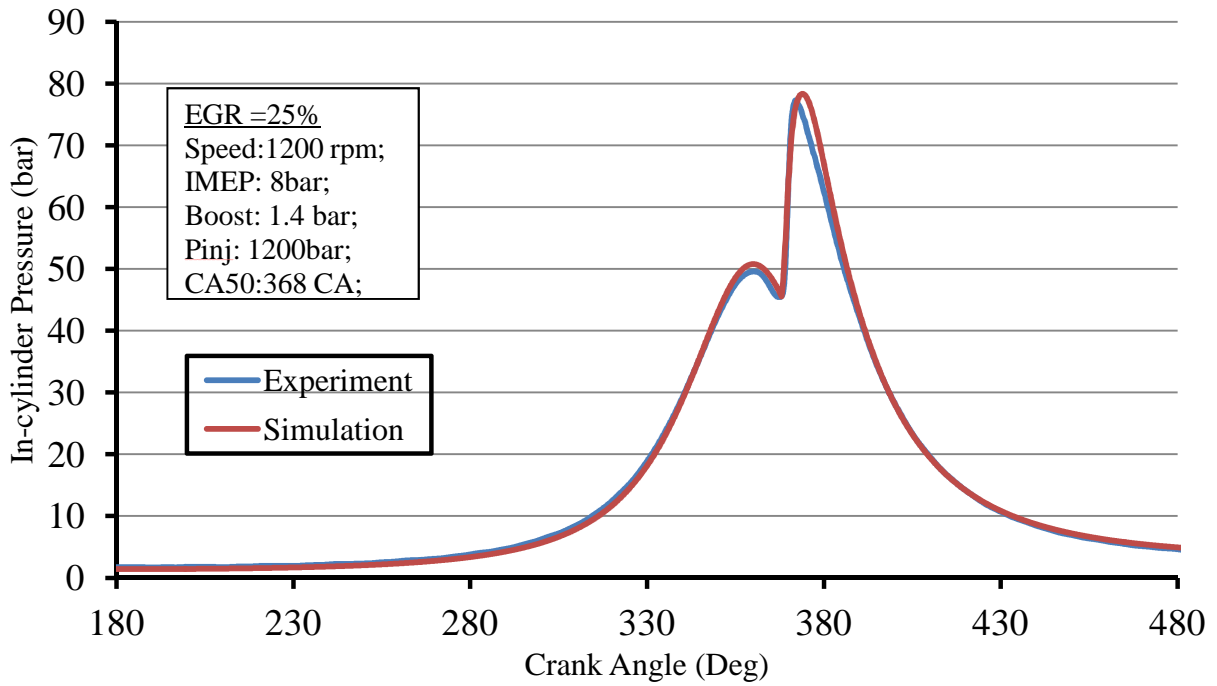


Figure A- 4 Comparison of the calculated and measured in-cylinder pressure (EGR=25%)

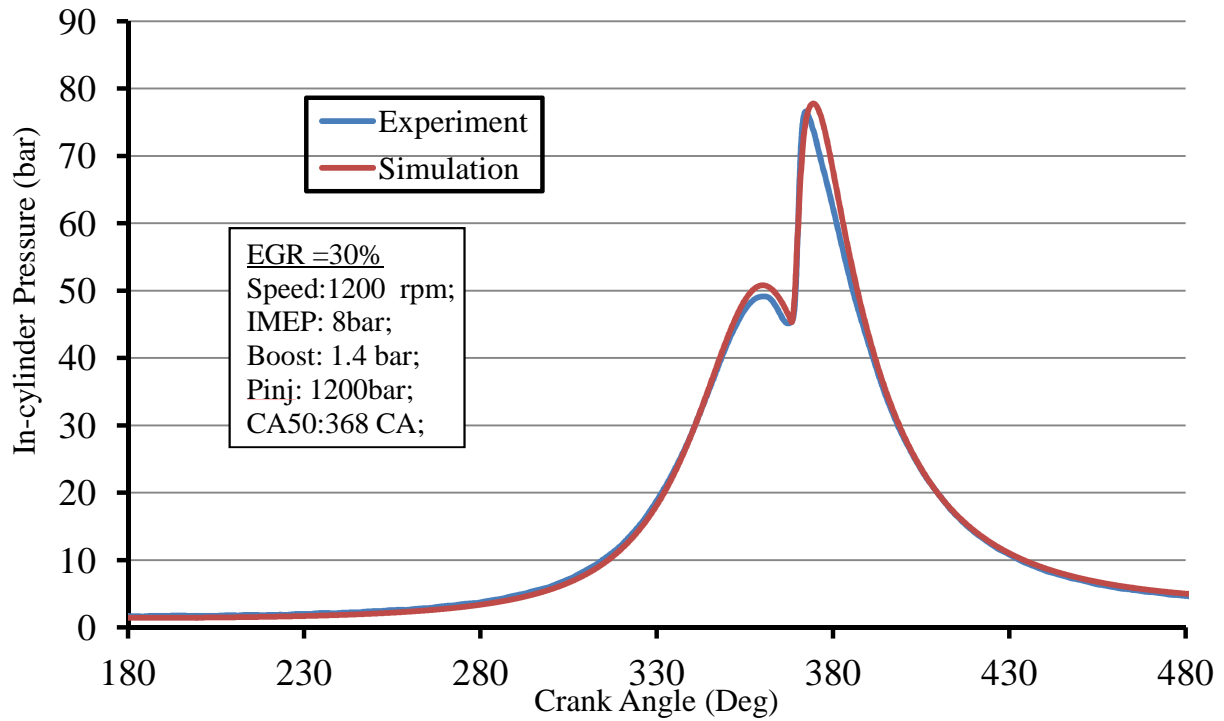


Figure A- 5 Comparison of the calculated and measured in-cylinder pressure (EGR=30%)

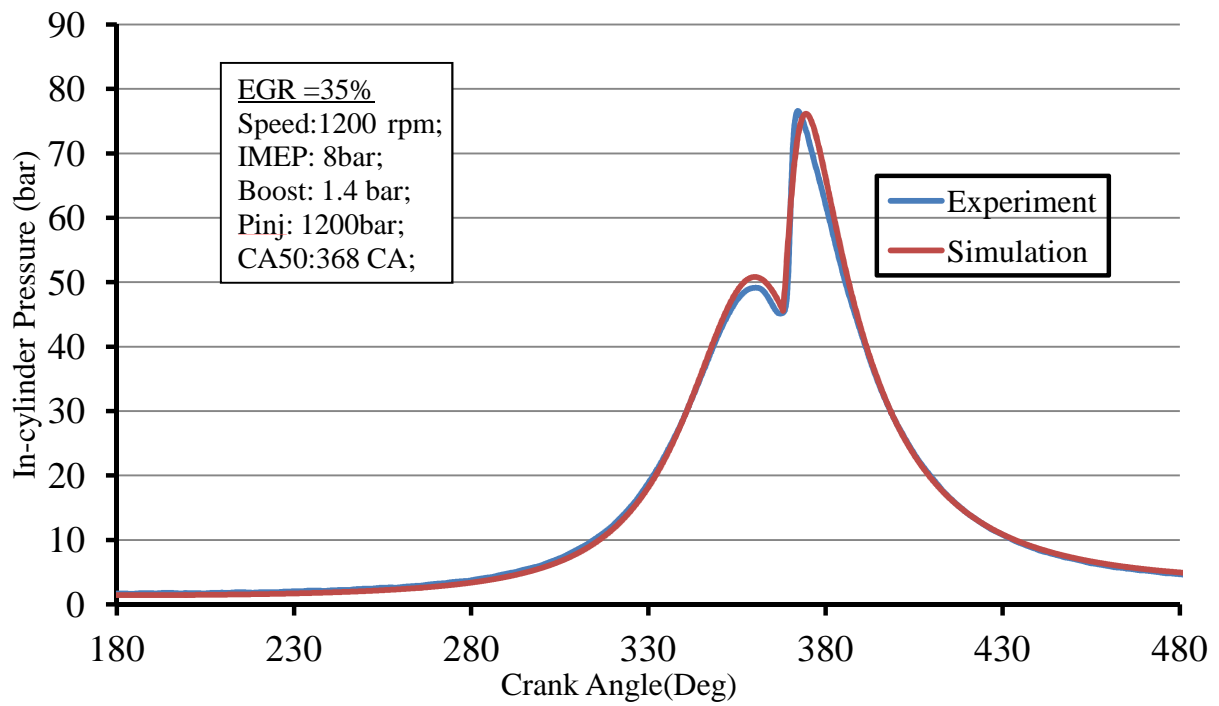


Figure A- 6 Comparison of the calculated and measured in-cylinder pressure (EGR=35%)



---

## VITA AUCTORIS

NAME: Fangfang Lin

PLACE OF BIRTH: Weihai, Shandong, P. R. China

EDUCATION: University of Windsor, Windsor, Ontario, Canada

2009-2011, M.A.Sc

Shandong University, Jinan, Shandong, P. R. China

2005-2008, M.A.Sc

Shandong University, Jinan, Shandong, P. R. China

2001-2005, B.Eng